

# A reinforcing HNF4-SMAD4 feed-forward module stabilizes enterocyte identity

Lei Chen<sup>1,2</sup>, Natalie H. Toke<sup>1</sup>, Shirley Luo<sup>1</sup>, Roshan P. Vasoya<sup>1</sup>, Robert L. Fullem<sup>1</sup>, Aditya Parthasarathy<sup>1</sup>, Ansu O. Perekatt<sup>3</sup> and Michael P. Verzi<sup>1,2\*</sup>

**BMP/SMAD signaling is a crucial regulator of intestinal differentiation<sup>1–4</sup>. However, the molecular underpinnings of the BMP pathway in this context are unknown. Here, we characterize the mechanism by which BMP/SMAD signaling drives enterocyte differentiation. We establish that the transcription factor HNF4A acts redundantly with an intestine-restricted HNF4 paralog, HNF4G, to activate enhancer chromatin and upregulate the majority of transcripts enriched in the differentiated epithelium; cells fail to differentiate on double knockout of both HNF4 paralogs. Furthermore, we show that SMAD4 and HNF4 function via a reinforcing feed-forward loop, activating each other's expression and co-binding to regulatory elements of differentiation genes. This feed-forward regulatory module promotes and stabilizes enterocyte cell identity; disruption of the HNF4-SMAD4 module results in loss of enterocyte fate in favor of progenitor and secretory cell lineages. This intersection of signaling and transcriptional control provides a framework to understand regenerative tissue homeostasis, particularly in tissues with inherent cellular plasticity<sup>5</sup>.**

Cellular identity arises from the combined activity of pioneer factors, which provide access to tissue-specific regulatory elements, and tissue-restricted transcription factors, which assemble at these accessible elements to control tissue-specific gene expression<sup>6</sup>. To define regulators of intestinal homeostasis, we employed assay for transposase accessible chromatin sequencing (ATAC-seq) to identify chromatin-accessible regions in the intestinal duodenal epithelium that are inaccessible in other tissues<sup>7</sup> (Supplementary Fig. 1a). We applied DNA-binding-motif analysis to identify transcription factors operating at these 4,575 intestine-specific regions (Supplementary Fig. 1a and Supplementary Table 1) and found that the hepatocyte nuclear factor 4 alpha/gamma (HNF4A/G) motif was the top-scoring factor, suggesting that HNF4 is a fundamental regulator of intestine-specific gene expression. HNF4A has been implicated prominently in the human genetics of inflammatory bowel disease<sup>8</sup> and colorectal cancer<sup>9,10</sup>. Chromatin immunoprecipitation–sequencing (ChIP-seq) studies have shown HNF4 can bind to differentiation genes; paradoxically, HNF4A is largely dispensable in the intestinal epithelium in mouse models<sup>11–13</sup>. We hypothesized that the extent and magnitude of HNF4A's functions have been masked by genetic redundancy with the paralog HNF4G, and further analysis<sup>7,14</sup> shows highly selective *Hnf4γ* expression in the intestine (Supplementary Fig. 1b–d). HNF4A and HNF4G also exhibited an overlapping immunofluorescence profile in the intestine (Fig. 1a). Using paralog-specific antibodies (Supplementary

Fig. 2a), we compared HNF4A and HNF4G binding with the intestinal epithelial genome using ChIP-seq. Strikingly similar binding profiles were observed (Fig. 1b and Supplementary Fig. 2b), with the vast majority of binding sites (98.7%) identified as common between HNF4A and HNF4G (7,193 sites, false discovery rate (FDR) < 0.05, DiffBind<sup>15</sup>; Fig. 1c and Supplementary Fig. 2c). HOMER analysis of HNF4A and HNF4G ChIP-seq-defined binding regions (Supplementary Fig. 2d) were enriched with nearly identical DNA-binding motifs, remarkably similar to previously defined HNF4 binding sequence preferences<sup>16</sup>. Taken together, the similar expression and DNA-binding profiles of the HNF4 paralogs justified further exploration of their possible genetic redundancy.

Although previous reports have indicated that *Hnf4g* (*Hnf4γ*) mutants are viable<sup>17,18</sup>, analysis of intestines lacking HNF4G is incomplete. We generated *Hnf4g*-knockout (*Hnf4γ*<sup>KO</sup>) mice via clustered regularly interspaced short palindromic repeats (CRISPR)-mediated editing (Supplementary Fig. 3a–c). Animals developed normally without HNF4G, were fertile, and showed no gross abnormalities in the histopathology or transcriptome of the intestine (Supplementary Fig. 3d–f). The relatively modest phenotype observed on loss of either HNF4A<sup>11–13,19</sup> or HNF4G indicated that these factors could function redundantly. We therefore generated double-mutant *Villin-Cre<sup>ERT2</sup>; Hnf4α<sup>fl</sup>; Hnf4γ<sup>CRISPR/CRISPR</sup>* mice. *Hnf4g* and *Hnf4a* double-knockout (*Hnf4αγ*<sup>DKO</sup>) adults showed rapid weight loss on tamoxifen treatment (Supplementary Fig. 4a) and had to be euthanized within 5 d, exhibiting fluid-filled intestines indicative of intestinal malfunction (Fig. 1d). Expression of differentiation markers, such as alkaline phosphatase and KRT20, indicated that differentiation was severely disrupted in the *Hnf4αγ*<sup>DKO</sup> mutants (Fig. 1e and Supplementary Fig. 4b,c). Dramatic expansion of the proliferation zone (Fig. 1f and Supplementary Fig. 4d,e) suggested that homeostatic balance was lost in the *Hnf4αγ*<sup>DKO</sup> mice, with expansion of the progenitor cell zone at the expense of cellular differentiation. Organoids derived from the *Hnf4αγ*<sup>DKO</sup> mutants grew in a manner consistent with an expansion of proliferative progenitors and a deficit of differentiated cells, with less debris in their lumens (Fig. 1g). Together, these findings reveal redundant functions between HNF4 paralogs in driving intestinal differentiation.

The molecular consequences of HNF4 redundancy were appreciated through transcriptome analysis. More than 2,892 genes were significantly altered in the *Hnf4αγ*<sup>DKO</sup> epithelium, whereas HNF4G or HNF4A loss yielded only 560 or 77 differentially expressed genes, respectively (FDR < 0.05, log<sub>2</sub>(fold change) > 1 or < −1) (Fig. 1h and Supplementary Fig. 4f). Genes downregulated in the *Hnf4αγ*<sup>DKO</sup>

<sup>1</sup>Department of Genetics, Human Genetics Institute of New Jersey, Rutgers University, Piscataway, NJ, USA. <sup>2</sup>Rutgers Cancer Institute of New Jersey, New Brunswick, NJ, USA. <sup>3</sup>Department of Chemistry and Chemical Biology, Stevens Institute of Technology, Hoboken, NJ, USA.

\*e-mail: [verzi@biology.rutgers.edu](mailto:verzi@biology.rutgers.edu)

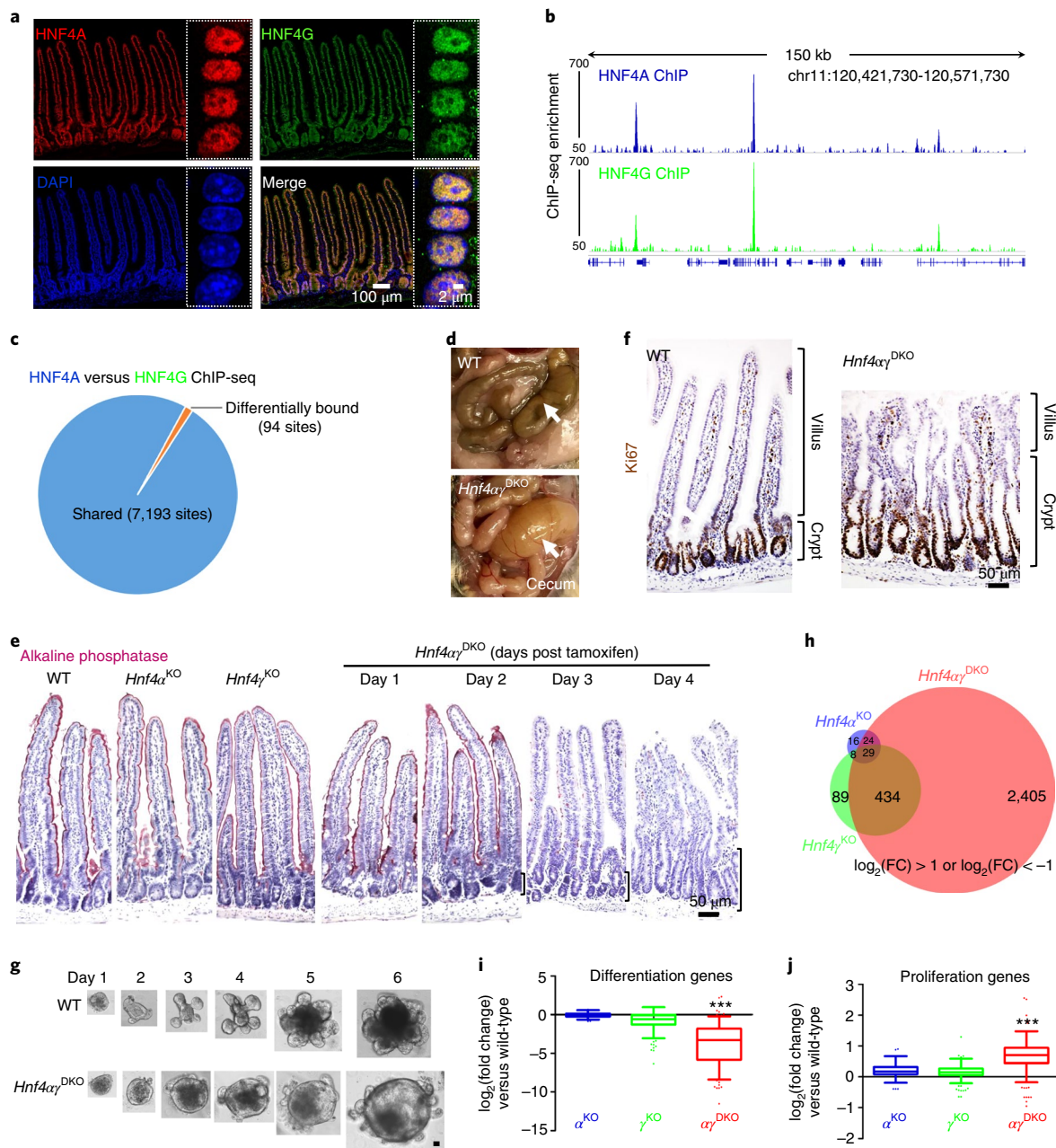


**Fig. 1 | HNF4A and HNF4G are redundantly required to drive intestinal differentiation.** **a**, Colocalization of HNF4A and HNF4G in intestinal epithelial cells by immunofluorescence confocal microscopy ( $n = 3$  biologically independent mice). The high-resolution images are of villus epithelial cell nuclei as shown in the boxed insets. ChIP-seq reveals strikingly similar binding profiles of HNF4A and HNF4G in the duodenal epithelial cells. **b**, Example of ChIP-seq tracks. **c**, DiffBind analysis (FDR  $< 0.05$ ;  $n = 2$  biologically independent mice) shows that 7,193 sites are shared and only 94 sites are differentially bound by HNF4A and HNF4G. Statistical tests were embedded in DiffBind. **d**, Necropsy reveals a distended and fluid-filled intestine in the *Hnf4 $\alpha\gamma$ <sup>DKO</sup>* mouse after 4 d of tamoxifen injection ( $n = 10$  independent experiments). Arrows highlight distended bowel. **e**, Alkaline phosphatase staining (differentiation marker, pink color,  $n = 4$  biologically independent mice). **f**, Immunostaining of Ki67 (proliferation marker, brown nuclei). Brackets show elongating crypts in the double mutants ( $n = 4$  biologically independent mice). The proliferation zone is defined by the distribution of Ki67<sup>+</sup> cells. **g**, In contrast with WT, *Hnf4 $\alpha\gamma$ <sup>DKO</sup>* organoids show a spherical morphology and fewer luminal contents, consistent with a failure to differentiate ( $n = 6$  independent experiments). Scale bar, 50  $\mu$ m. **h**, Only *Hnf4 $\alpha\gamma$ <sup>DKO</sup>* mice show a striking alteration of gene expression as evidenced by RNA-seq ( $n = 3$  biologically independent mice). Venn diagram shows the numbers of genes in HNF4 single and double mutants with  $\log_2(\text{fold change}) > 1$  or  $< -1$ , FDR  $< 0.05$ . Statistical tests were embedded in Cuffdiff. **i, j**, Differentiation genes (**i**) are reduced, whereas proliferation genes (**j**) are elevated in the *Hnf4 $\alpha\gamma$ <sup>DKO</sup>* mice. The middle line represents the median; whiskers represent the tenth and ninetieth percentiles. Post hoc Dunn's test was applied following a Kruskal-Wallis test at \*\*\* $P < 0.001$  ( $n = 3$  biologically independent mice). DKO, double knockout; FC, fold change.

mutants were enriched for ontologies associated with enterocyte functions in digestive metabolism, enterocyte morphology and immune signaling (Supplementary Fig. 4g). The number of gene expression changes and their magnitude in the double mutant

(Fig. 1h and Supplementary Fig. 4f), versus relatively subtle differences in the single mutants (Supplementary Fig. 5), suggest largely redundant functions between HNF4 factors. *Hnf4 $\alpha\gamma$ <sup>DKO</sup>* epithelium exhibited a robust shift in the transcriptome away from

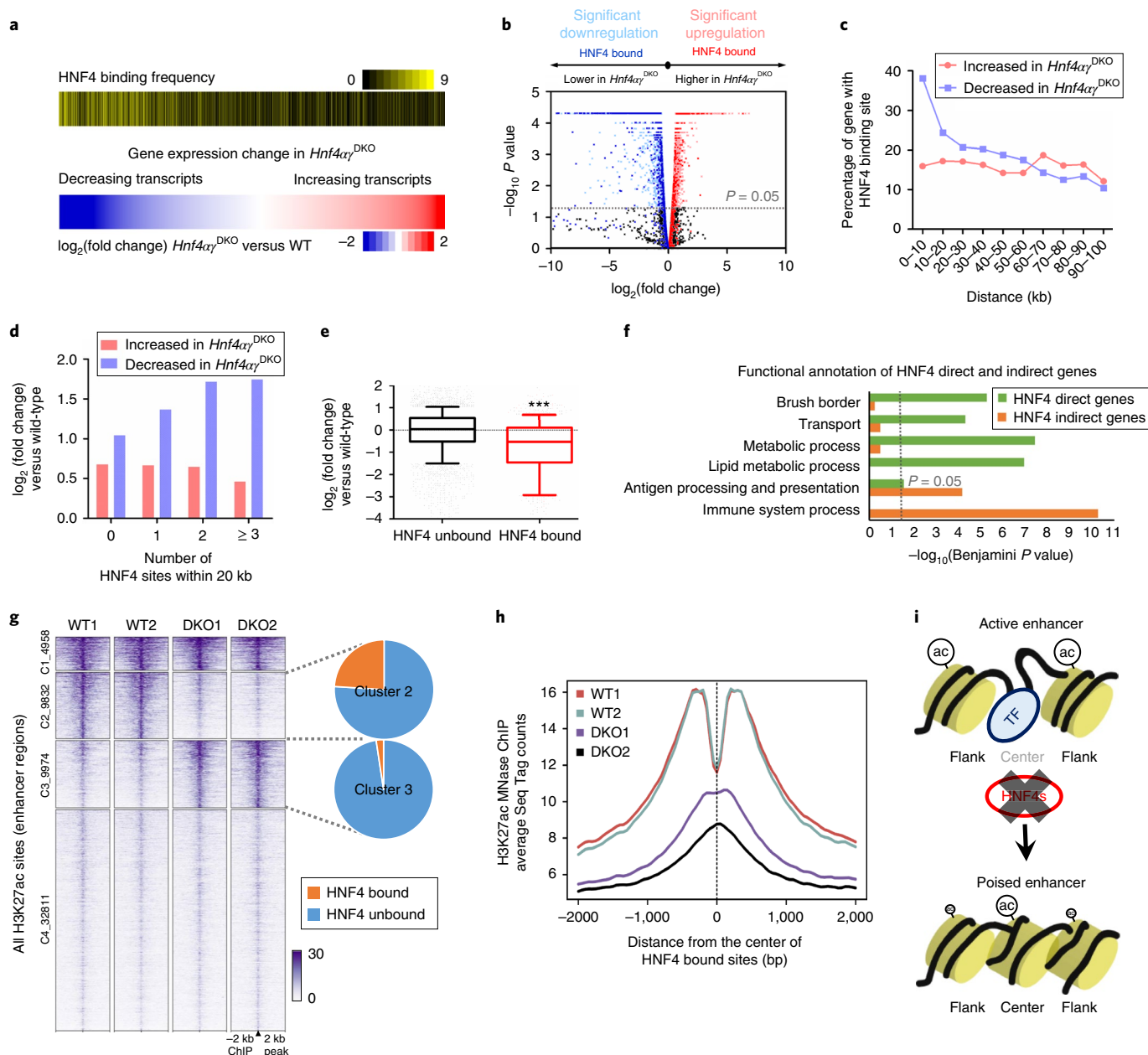


**Fig. 2 | HNF4 binding is required to activate enhancer chromatin and stimulate genes required for intestinal differentiation.** **a**, HNF4 factors function primarily to activate rather than repress transcription, as evidenced by heat maps (Kolmogorov–Smirnov test, one-sided for positive and negative enrichment scores,  $P < 0.001$ ). The lower heat map displays a  $\log_2(\text{fold change})$  in gene expression ( $n = 3$  biologically independent mice). The upper heat map shows the corresponding frequency (yellow shading) of HNF4-binding sites located within 20 kb of the TSSs of the corresponding genes in 10-gene binned groups displayed in the expression heat map. **b**, Volcano plot of gene expression changes ( $n = 3$  biologically independent mice). Significant genes were called via Cuffdiff. **c**, Distribution of TSS distances in 10 kb windows from the nearest HNF4-binding sites. Genes with an FDR  $< 0.05$  are determined as either decreased or increased in the *Hnf4α<sup>DKO</sup>* duodenum compared with the controls ( $n = 3$  biologically independent mice). Downregulated genes are more likely to have nearby HNF4-binding sites than upregulated genes. **d**, Genes that decrease in HNF4-deficient epithelium are more likely to harbor multiple HNF4 binding events than genes that show increased expression ( $n = 3$  biologically independent mice). **e**, HNF4-bound genes are significantly downregulated in *Hnf4α<sup>DKO</sup>* compared with unbound genes. The middle line represents the median; whiskers represent the tenth and ninetieth percentiles (Mann–Whitney  $U$ -test, two-sided at  $***P < 0.001$ ;  $n = 3$  biologically independent mice). **f**, Functional annotation of HNF4 direct and indirect genes ( $\log_2(\text{fold change}) < -1$ ; FDR  $< 0.05$ ) by DAVID. Direct genes: HNF4-bound genes (genes within 30 kb of annotated TSSs nearby HNF4-binding sites). Indirect genes: HNF4-unbound genes. Benjamini  $P$  values were calculated using DAVID. **g**, MNase–ChIP-seq profiles ( $k$ -means = 4; MACS  $P \leq 10^{-5}$ ) of H3K27ac. Statistical tests were embedded in the MACS package. **h**, Aggregate plots of H3K27ac ChIP-seq signal are centered on the 5,952 enhancer sites that are bound by HNF4, and loss of HNF4 paralogs prominently reduces H3K27ac signal. **i**, Model of HNF4 control of active chromatin structures in the intestine. DKO, double knockout; TSSs, transcription start sites.

differentiated cell transcripts<sup>20</sup> and toward proliferating cell transcripts<sup>20</sup> (Fig. 1i,j, Supplementary Fig. 4h and Supplementary Table 2).

Nearly 45% of genes with reduced expression in the *Hnf4α<sup>DKO</sup>* intestines showed binding of HNF4 within 20 kb, which implies that

HNF4 factors directly transactivate these genes. Conversely, genes upregulated on loss of both HNF4 paralogs showed no significant enrichment of binding by HNF4 factors (Fig. 2a,b), suggesting that HNF4 binds and activates enterocyte differentiation genes and



indirectly suppresses crypt/proliferation (examples are illustrated in Supplementary Fig. 4i). Association between HNF4 binding and linked gene expression diminished with distance (Fig. 2c), and the frequency of HNF4 binding events at a gene correlated to the magnitude of linked gene expression changes (Fig. 2d). Expression of HNF4-bound genes showed greater changes in transcript levels than unbound genes in *Hnf4a*<sup>DKO</sup> (Fig. 2e). Gene ontology analysis revealed that HNF4 direct-target genes (1,036 genes with log<sub>2</sub>(fold change) < -1 and FDR < 0.05, within 30 kb of HNF4-binding sites) function in processes typical of differentiated enterocytes, whereas downregulated genes lacking HNF4-binding sites were more enriched in immune-related functions, suggesting an indirect role for HNF4 factors (Fig. 2f). HNF4-binding regions also exhibited properties of transcriptional enhancers, including ChIP-seq enrichment for chromatin features and coregulators typically found at enhancers (Supplementary Fig. 6a,b). To explore how HNF4 factors were activating differentiation genes, we profiled enhancer chromatin structures in control and *Hnf4a*<sup>DKO</sup> mutants using H3K27ac-micrococcal nuclease (MNase)-ChIP-seq. HNF4 binding was most abundant at regions losing H3K27ac signal in the *Hnf4a*<sup>DKO</sup> (9,832 sites, 24.0% of which bind HNF4), whereas regions gaining H3K27ac signal showed the least HNF4 binding (9,974 sites, 2.4% of which bind HNF4; Fig. 2g). This suggests that HNF4 factors function to maintain active enhancer chromatin, but not to directly repress chromatin. H3K27ac signal was observed at nucleosomes flanking HNF4-binding sites in control mice, and this pattern was disrupted on loss of HNF4 factors (Fig. 2h,i). Conversely, H3K27ac levels at promoters were unaffected in the *Hnf4a*<sup>DKO</sup> mutants (Supplementary Fig. 6c). These findings indicate that HNF4 drives differentiation by activating gene expression in the intestinal epithelium through binding to distal enhancer regions and maintaining enhancer chromatin activity.

BMP/SMAD signaling is well recognized as a driver of intestinal differentiation<sup>1-4</sup>, although its molecular mechanisms are unclear. Given HNF4's potent role in driving the differentiation program (Figs. 1 and 2 and Supplementary Fig. 7), we wondered whether HNF4 and BMP/SMAD could be working in concert. Highly similar transcriptome changes occurred on loss of the BMP-effector transcription factor SMAD4 and in our *Hnf4a*<sup>DKO</sup> model, suggesting that these factors could be working in the same pathway (Fig. 3a). Interestingly, transcripts of SMAD factors and BMP ligands were dramatically reduced on HNF4 loss in the epithelium (FDR < 0.001; Fig. 3b). Phosphorylated SMAD1/5/9 and total protein level of SMAD4 and SMAD5 were also diminished in the nucleus of villus epithelial cells from *Hnf4a*<sup>DKO</sup> (Fig. 3c-e). Consistent with direct

activation by HNF4, active chromatin was lost at HNF4-bound regions of *Smad4*, *Smad5* and *Bmp1* loci of *Hnf4a*<sup>DKO</sup> (Fig. 3f and Supplementary Fig. 8a). These findings suggest that HNF4 directly activates BMP/SMAD signaling.

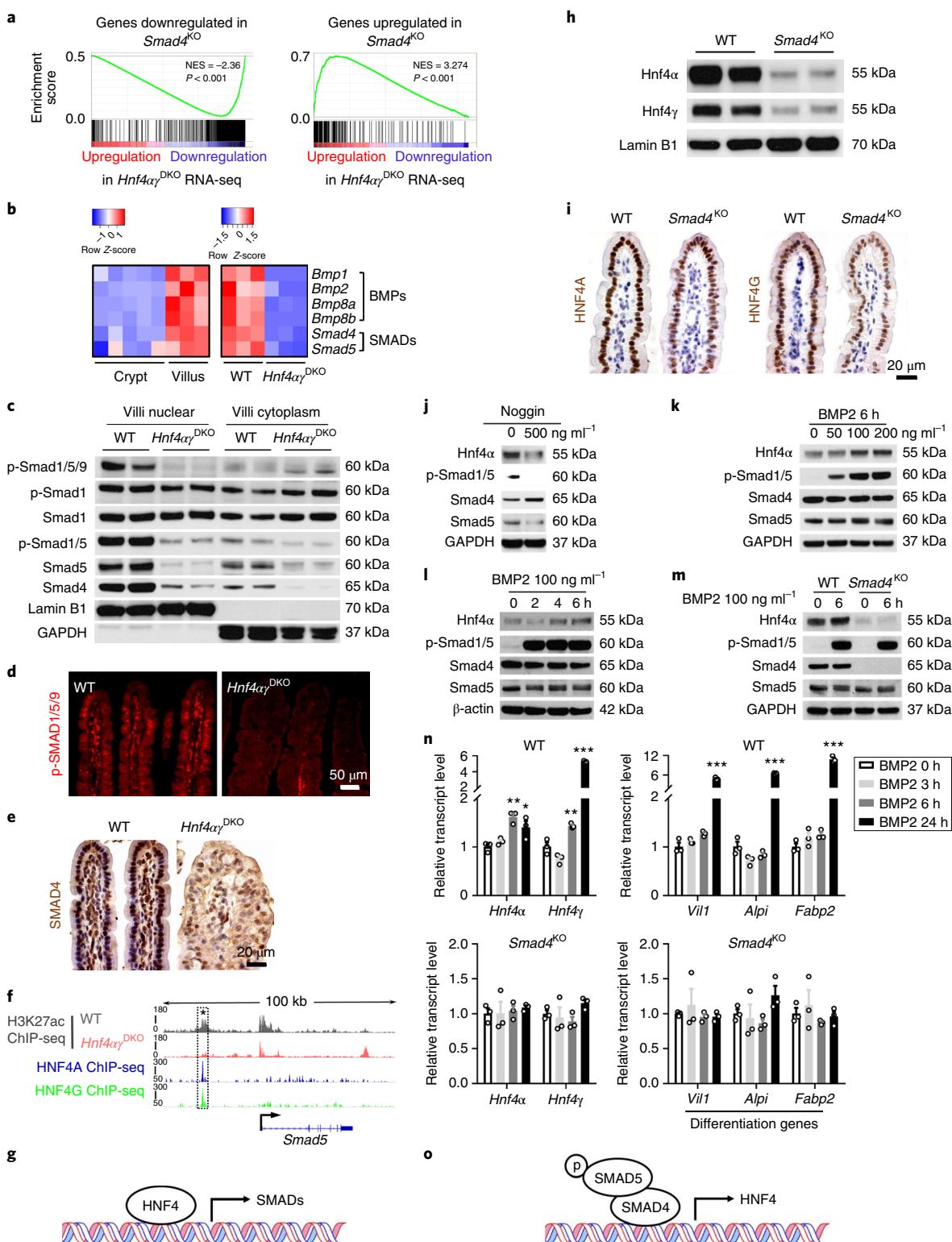
Positive feedback mechanisms can stabilize cellular lineage decisions<sup>21</sup>, and we investigated whether BMP signaling reciprocally stimulates HNF4 expression. Reduced *Hnf4a* and *Hnf4y* transcript and protein levels (Fig. 3h,i and Supplementary Fig. 8b) were found in the villi of *Smad4*<sup>KO</sup> mice. In primary intestinal organoids, HNF4A protein levels were suppressed after addition of the BMP antagonist Noggin, but elevated by BMP2 treatment (Fig. 3j-l). HNF4G expression was also responsive to BMP2 treatment (Supplementary Fig. 8c,d), consistent with redundancy of *Hnf4a* and *Hnf4y*. BMP signaling suppressed stem cell genes (Supplementary Fig. 8e) as previously reported<sup>22</sup>, but also promoted enterocyte differentiation genes (Fig. 3n). BMP2-mediated activation of HNF4 protein and transcripts was dependent on SMAD4, because the responses were not observed in *Smad4*<sup>KO</sup> tissues (Fig. 3m,n). *Hnf4a* expression was elevated as early as 6 h after treatment with BMP2 ligand, whereas enterocyte differentiation markers were not elevated until 24 h (Fig. 3n and Supplementary Fig. 8f), suggesting that *Hnf4a* is an early target of BMP signaling.

These data indicate a feed-forward differentiation mechanism in which HNF4 transcription factors and BMP/SMAD signaling reciprocally activate each other's expression in intestinal villi (Fig. 3g,o). Such a regulatory relationship could then impart a differentiation program by activating intermediary differentiation factors or by directly activating a larger cadre of prodifferentiation transcripts. We explored the downstream activities of these two factors using ChIP-seq and RNA-seq in both mouse and human model systems. ChIP-seq of SMAD4 and HNF4A<sup>23</sup> in Caco-2 cells indicated a broad regulatory partnership, with more than 18,000 genomic regions commonly targeted by both HNF4A and SMAD4 factors (47% of SMAD4-binding sites; Fig. 4a). Canonical SMAD4 and HNF4A/G motifs were enriched at these regions (Fig. 4b), suggesting that many of these regions were co-occupied by SMAD4 and HNF4. HNF4A and SMAD4 shared regulatory regions present at the *HNF4A* (Fig. 4c) and *SMAD5* (Fig. 4d) loci, consistent with the reciprocal activation between HNF4 and SMAD4 seen in mice. Colocalized binding of HNF4A and SMAD4 was observed at a number of enterocyte-specific genes (Fig. 4e). Overlapping expression (Supplementary Fig. 8g) and co-binding of genomic enhancers of HNF4 and SMAD4 were also observed in ChIP-seq on mouse intestinal epithelium (Fig. 4f-h). At the transcriptome level, the 541 genes that were significantly downregulated both in the *Smad4*<sup>KO</sup> and

**Fig. 3 | HNF4 and BMP/SMAD reinforce each other's expression. a-g**, HNF4 binds and activates core components of the BMP/SMAD signaling pathways. **a**, GSEA reveals that genes downregulated or upregulated on SMAD4 loss strongly correlate with genes of reduced expression or increased expression in *Hnf4a*<sup>DKO</sup>, respectively (Kolmogorov-Smirnov test, one-sided for positive and negative enrichment scores,  $P < 0.001$ ;  $n = 3$  biologically independent mice). **b**, Heat map displays that RNA-seq expression levels of BMPs/SMADs are highly expressed in villus compared with the crypt and are significantly reduced in the *Hnf4a*<sup>DKO</sup> intestinal epithelium compared with the WT littermate controls ( $n = 3$  biologically independent mice; FDR < 0.001). Statistical tests were embedded in Cuffdiff. **c**, This is also evidenced by western blot ( $n = 2$  independent experiments and 2 biologically independent mice for each experiment). **d,e**, Immunofluorescence staining of p-SMAD1/5/9 (**d**) and immunohistochemistry staining of SMAD4 (**e**) also show reduced levels on HNF4 loss (representative of three biologically independent mice). **f**, ChIP-seq tracks ( $n = 2$  biologically independent mice) show that HNF4 factors bind to *Smad5*, and loss of HNF4 results in reduced H3K27ac signal (see dashed rectangles). Reciprocally, HNF4 levels are dependent on BMP/SMAD4. **h-o**, BMP/SMAD signaling promotes HNF4 expression. **h,i**, Western blot ( $n = 2$  independent experiments and 2 biologically independent mice for each experiment) (**h**) and immunostaining ( $n = 3$  biologically independent mice) (**i**) show that SMAD4 knockout (4 d after tamoxifen injection) can cause significant downregulation of nuclear protein levels of *Hnf4a* and *Hnf4y* in the villi. **j-l**, Western blot of the primary WT intestinal organoids in the presence of (**j**) Noggin treatment (BMP antagonist, 72 h,  $n = 2$  independent experiments), (**k**) 6 h treatment of different dosages of BMP2 ( $n = 3$  independent experiments), and (**l**) different durations of BMP2 treatment ( $n = 3$  independent experiments). **m**, BMP2 can induce *Hnf4a* expression in the primary WT intestinal organoids, but this effect is abolished in the absence of *Smad4* ( $n = 2$  independent experiments). Uncropped western blots are shown in Supplementary Fig. 11. **n**, qRT-PCR shows that BMP2 (100 ng ml<sup>-1</sup>) promotes *Hnf4* and differentiation gene expression in the primary WT intestinal organoids, but not in the *Smad4*<sup>KO</sup> organoids. All of the qPCR data are presented as mean  $\pm$  s.e.m. ( $n = 3$  independent organoid cultures). Transcript levels relative to BMP 0 h and statistical comparisons were performed using one-way ANOVA followed by Dunnett's posttest at \*\*\* $P < 0.001$ , \*\* $P < 0.01$  and \* $P < 0.05$ . All of the primary organoids were harvested at day 6 after seeding. DKO, double knockout; NES, normalized enrichment score.

*Hnf4α*<sup>DKO</sup> mice (Fig. 4i and Supplementary Fig. 8h) were associated with enterocyte functions such as lipid metabolism, microvillus and absorption. Conversely, genes downregulated only in *Hnf4α*<sup>DKO</sup> and not in *Smad4*<sup>KO</sup> were more associated with generalized ontologies of cytoplasm and Golgi apparatus (Fig. 4j and Supplementary Table 3). These findings suggest that the convergence of SMAD4 and HNF4 is critical to achieve a robust, enterocyte-specific gene expression program.

Our findings identify a reinforcing regulatory loop between the transcription factors HNF4 and SMAD4. Loss of this regulatory loop could impair enterocyte differentiation and/or destabilize enterocyte identity. Indeed, we observed a bias toward crypt cell structures and gene expression when loss of HNF4 factors (Fig. 1). In addition, a clear shift in the transcriptome occurred away from enterocyte transcripts<sup>24</sup> and toward secretory goblet cell transcripts<sup>24</sup> upon HNF4 loss (Fig. 5a–c and Supplementary Table 2), and goblet



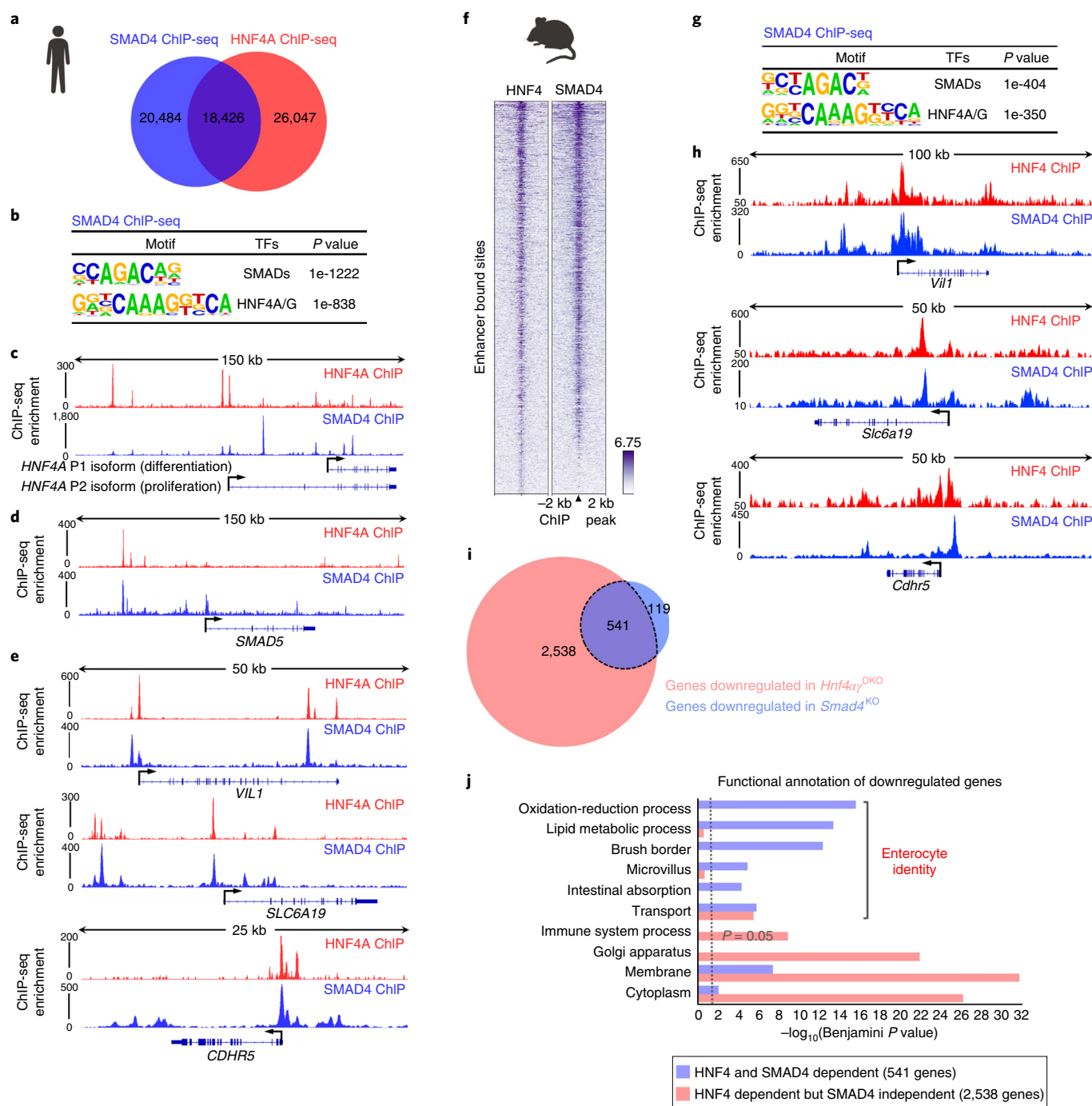


**Fig. 4 | HNF4 and SMAD4 cobind genomic enhancers, activating enterocyte identity genes.** One replicate of the human Caco-2 cell line and two replicates of biologically independent mouse tissues were used in ChIP-seq analysis. Statistical tests were embedded in MACS and HOMER. **a,b**, ChIP-seq in Caco-2 cells reveals that SMAD4 and HNF4A cobind genomic regions, as evidenced by Venn diagram (MACS  $P \leq 10^{-5}$ ) (**a**) and HOMER motif analysis (MACS  $P \leq 10^{-10}$ ) (**b**). **c–e**, HNF4A and SMAD4 bind to gene loci of *HNF4A* (**c**), *SMAD5* (**d**) and enterocyte differentiation genes (*VIL1*, *SLC6A19* and *CDHR5*) (**e**) in Caco-2 cells. ChIP-seq in mouse intestinal epithelium also reveals that SMAD4 and HNF4 cobind genomic regions ( $n = 2$  biologically independent mice each). **f**, Heat map shows a similar binding pattern of SMAD4 (MACS  $P \leq 10^{-5}$ ) and HNF4 (MACS  $P \leq 10^{-3}$ ) at their enhancer bound sites. **g**, HOMER motif analysis of mouse SMAD4 ChIP-seq (MACS  $P \leq 10^{-5}$ , enhancer sites). **h**, HNF4 and SMAD4 cobind to enterocyte differentiation genes (*Vil1*, *Slc6a19* and *Cdhr5*) in mouse intestinal epithelium. **i**, Venn diagram shows highly overlapping target genes with significant downregulation (FDR  $< 0.05$ ) in the intestine of *Hnf4a*<sup>DKO</sup> (red circle) and genes with significant downregulation (FDR  $< 0.05$ ) in *Smad4*<sup>KO</sup> (blue circle). Significant genes were called via Cuffdiff ( $n = 3$  biologically independent mice). **j**, Enterocyte-related functions are enriched among HNF4–SMAD4 codependent genes (common downregulated genes, 541 genes, purple bars) compared with genes downregulated in only *Hnf4a*<sup>DKO</sup>, but not in *Smad4*<sup>KO</sup> (2,538 genes, red bars). This suggests the combined functions of HNF4 and SMAD4 are specifically driving the transcriptome toward enterocyte identity. Benjamini  $P$  values were calculated using DAVID. DKO, double knockout.



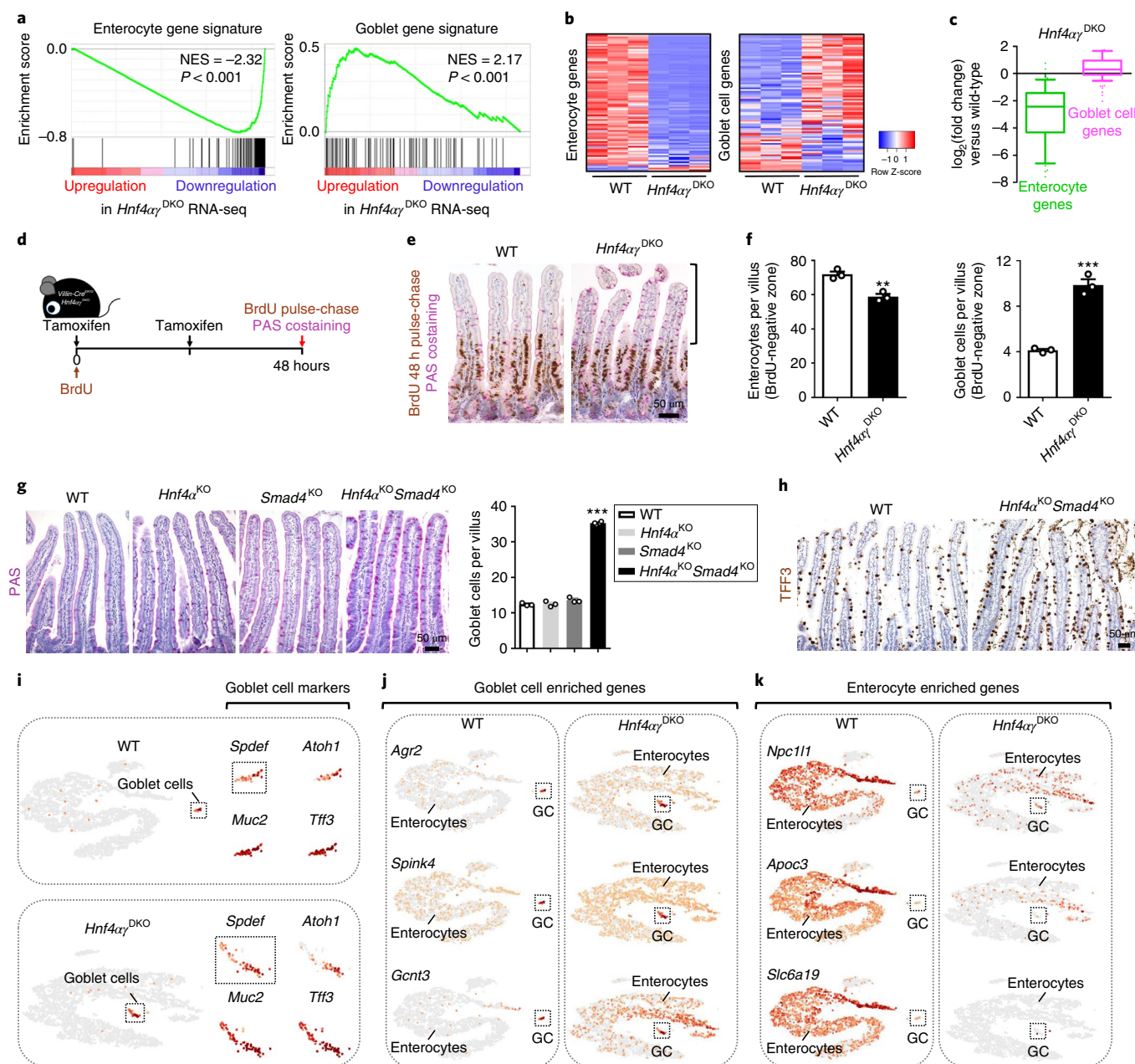


**Fig. 5 | Disruption of an HNF4-SMAD4 regulatory loop compromises enterocyte identity.** **a**, GSEA of RNA-seq data ( $n=3$  biologically independent mice) reveals that the transcriptome moves away from enterocyte transcripts and toward secretory goblet cell transcripts on HNF4 loss (Kolmogorov-Smirnov test, one-sided for positive and negative enrichment scores,  $P < 0.001$ ). **b,c**, Heat maps (**b**) and box plots (**c**) show that enterocyte signature transcripts are reduced, whereas goblet cell signature transcripts are elevated in  $Hnf4\alpha^{DKO}$ . The middle line represents the median; whiskers represent the tenth and ninetieth percentiles (Mann-Whitney  $U$ -test, two-sided,  $P < 0.001$ ;  $n=3$  biologically independent mice). **d**, Schematic of BrdU pulse-chase and PAS costaining experiment. **e**, Costaining of BrdU (48 h pulse-chase) and PAS. **f**, Enterocytes (PAS<sup>-</sup>) and goblet cells (PAS<sup>+</sup>) were counted within the BrdU<sup>-</sup> zone of 50 villi per mouse. The data are presented as mean  $\pm$  s.e.m. ( $n=3$  biologically independent mice, Student's  $t$ -test, two-sided at \*\*\* $P < 0.001$  and \*\* $P < 0.01$ ). **g**, Mice were injected with tamoxifen for four consecutive days and harvested 10 d after the first injection. Goblet cells were counted on 30 villi per mouse (WT and single mutants:  $n=3$  biologically independent mice; double mutants:  $n=4$  biologically independent mice; one-way ANOVA followed by Dunnett's posttest at \*\*\* $P < 0.001$ ). **h**, Goblet cell markers are elevated in mutants as evidenced by immunohistochemistry staining of TFF3 ( $n=3$  biologically independent mice). **i-k**, Single-cell RNA-seq on dissociated villus epithelium. Canonical goblet cell markers were used to identify goblet cell clusters (**i**) in WT and mutants. Compared with WT, goblet cell-enriched genes are increased (**j**), whereas enterocyte-enriched genes are decreased (**k**) in the enterocyte clusters of mutants, suggesting compromised enterocyte identity. Estimated number of cells in each experiment was WT:  $n=4,100$  and  $Hnf4\alpha^{DKO}$ :  $n=4,200$ . DKO, double knockout; NES, normalized enrichment score; GC, goblet cells.

cell numbers increased in  $Hnf4\alpha^{DKO}$  (Supplementary Fig. 9a–c). To help discern whether HNF4 is required for enterocyte differentiation and/or fate stability, we monitored villus-resident enterocytes in  $Villin-Cre^{ERT2}; Hnf4\alpha^{DKO}$  and their littermate controls. We labeled

proliferating cells by using 5-bromodeoxyuridine (BrdU) at the time of tamoxifen-induced genetic changes and monitored enterocyte fate at 48 h posttreatment (Fig. 5d). In this assay, we assumed all cells above the BrdU<sup>+</sup> zone represented cells that were postmitotic

and had already migrated out of the crypt at the time of co-treatment with BrdU and tamoxifen to induce the loss of HNF4. These postmitotic cells in the *Hnf4a*<sup>DKO</sup> mice were more likely to exhibit features of secretory goblet cells than littermate controls (Fig. 5e). One possible explanation for the increased numbers of goblet cells could be that enterocytes are converting to goblet cells in the absence of HNF4 factors. Alternatively, the increase in goblet cell numbers could be attributed to conversion of other cell populations in the villus or rapid migration of nondividing goblet progenitor crypt cells toward villus tips. However, given that there appears to be a loss of enterocyte numbers above the BrdU<sup>+</sup> zone that is proportional to the increased number of goblet cells gained (Fig. 5f), and no significant difference in the number of goblet cells in the crypts (Supplementary Fig. 9d), we favor the interpretation that cells are undergoing an enterocyte-to-goblet conversion. Consistent with a coregulatory relationship between HNF4 and SMAD4, combined loss of SMAD4 and HNF4A also led to accumulation of goblet cells (Fig. 5g,h and Supplementary Fig. 9e).

The coincident increase in goblet cells and decrease in enterocytes within the postmitotic zone of the villi suggested that enterocytes could be converting toward a goblet cell identity (Fig. 5a–h). To further explore this possibility, we applied single-cell RNA-seq to control and mutant villus epithelial cells. Goblet cells were distinguished from enterocytes by canonical goblet cell markers (*Spdef*, *Atoh1*, *Muc2* and *Tff3*) and were clearly identified in the dissociated villus cells of control, *Hnf4a*<sup>DKO</sup> and *Hnf4a*<sup>KO</sup>; *Smad4*<sup>KO</sup>, respectively (Fig. 5i and Supplementary Fig. 9f). Goblet cell-enriched genes<sup>24</sup>, such as *Agr2*, *Spink4*, *Gcnt3* and *S100a6*, were highly expressed in the goblet cell clusters of WT, *Hnf4a*<sup>DKO</sup> and *Hnf4a*<sup>KO</sup>; *Smad4*<sup>KO</sup>, but were also expressed in the enterocyte clusters of mutants (Fig. 5j and Supplementary Fig. 9g). Conversely, enterocyte-enriched genes<sup>24,25</sup>, such as *Npc1l1*, *Apoc3*, *Slc6a19* and *Lct*, were reduced in the enterocyte clusters of *Hnf4a*<sup>DKO</sup> and *Hnf4a*<sup>KO</sup>; *Smad4*<sup>KO</sup> compared with WT (Fig. 5k and Supplementary Fig. 9h). Thus, the majority of enterocytes in these mutant models exhibited a mixed expression profile, featuring ectopic levels of goblet cell-enriched transcripts and diminished levels of enterocyte-enriched transcripts. Taken together, these data suggest that the BMP/SMAD signaling pathway promotes differentiation via HNF4 transcription factors, and together, they stabilize enterocyte identity via a positive regulatory loop (Supplementary Fig. 10). Disruption of the HNF4–SMAD4 feed-forward circuit results in loss of enterocyte fate in favor of progenitor (Fig. 1) and goblet cell (Fig. 5) identities. Thus, the reinforcing regulatory module identified in this work may be especially important for enterocyte differentiation and lineage stability in a tissue with an underlying permissive chromatin environment<sup>5,26,27</sup>. The HNF4–SMAD4 regulatory model also predicts hurdles that must be overcome in order for enterocytes to exit their differentiated state and contribute to regenerative or oncogenic programs.

### Online content

Any methods, additional references, Nature Research reporting summaries, source data, statements of data availability and associated accession codes are available at <https://doi.org/10.1038/s41588-019-0384-0>.

Received: 11 June 2018; Accepted: 28 February 2019;  
Published online: 15 April 2019

### References

- Davis, H. et al. Aberrant epithelial GREM1 expression initiates colonic tumorigenesis from cells outside the stem cell niche. *Nat. Med.* **21**, 62–70 (2015).
- Haramis, A. P. et al. De novo crypt formation and juvenile polyposis on BMP inhibition in mouse intestine. *Science* **303**, 1684–1686 (2004).
- He, X. C. et al. BMP signaling inhibits intestinal stem cell self-renewal through suppression of Wnt-beta-catenin signaling. *Nat. Genet.* **36**, 1117–1121 (2004).
- Auclair, B. A., Benoit, Y. D., Rivard, N., Mishina, Y. & Perreault, N. Bone morphogenetic protein signaling is essential for terminal differentiation of the intestinal secretory cell lineage. *Gastroenterology* **133**, 887–896 (2007).
- Kim, T. H. et al. Broadly permissive intestinal chromatin underlies lateral inhibition and cell plasticity. *Nature* **506**, 511–515 (2014).
- Iwafuchi-Doi, M. & Zaret, K. S. Cell fate control by pioneer transcription factors. *Development* **143**, 1833–1837 (2016).
- Vierstra, J. et al. Mouse regulatory DNA landscapes reveal global principles of cis-regulatory evolution. *Science* **346**, 1007–1012 (2014).
- UK IBD Genetics Consortium, et al. Genome-wide association study of ulcerative colitis identifies three new susceptibility loci, including the HNF4A region. *Nat. Genet.* **41**, 1330–1334 (2009).
- Cancer Genome Atlas Network. Comprehensive molecular characterization of human colon and rectal cancer. *Nature* **487**, 330–337 (2012).
- Zhang, B. et al. Proteogenomic characterization of human colon and rectal cancer. *Nature* **513**, 382–387 (2014).
- Babeu, J. P., Darsigny, M., Lussier, C. R. & Boudreau, F. Hepatocyte nuclear factor 4alpha contributes to an intestinal epithelial phenotype in vitro and plays a partial role in mouse intestinal epithelium differentiation. *Am. J. Physiol. Gastrointest. Liver Physiol.* **297**, G124–G134 (2009).
- Cattin, A. L. et al. Hepatocyte nuclear factor 4alpha, a key factor for homeostasis, cell architecture, and barrier function of the adult intestinal epithelium. *Mol. Cell Biol.* **29**, 6294–6308 (2009).
- San Roman, A. K., Aronson, B. E., Krasinski, S. D., Shivdasani, R. A. & Verzi, M. P. Transcription factors GATA4 and HNF4A control distinct aspects of intestinal homeostasis in conjunction with transcription factor CDX2. *J. Biol. Chem.* **290**, 1850–1860 (2015).
- Lin, S. et al. Comparison of the transcriptional landscapes between human and mouse tissues. *Proc. Natl Acad. Sci. USA* **111**, 17224–17229 (2014).
- Stark, R. & Brown, G. D. DiffBind: differential binding analysis of ChIP-seq peak data. *Bioconductor* <http://bioconductor.org/packages/release/bioc/html/DiffBind.html> (2011).
- Fang, B., Mane-Padros, D., Bolotin, E., Jiang, T. & Sladek, F. M. Identification of a binding motif specific to HNF4 by comparative analysis of multiple nuclear receptors. *Nucl. Acids Res.* **40**, 5343–5356 (2012).
- Gerdin, A. K. et al. Phenotypic screening of hepatocyte nuclear factor (HNF) 4-gamma receptor knockout mice. *Biochem. Biophys. Res. Commun.* **349**, 825–832 (2006).
- Baraille, F. et al. Glucose tolerance is improved in mice invalidated for the nuclear receptor HNF-4gamma: a critical role for enteroendocrine cell lineage. *Diabetes* **64**, 2744–2756 (2015).
- Verzi, M. P., Shin, H., San Roman, A. K., Liu, X. S. & Shivdasani, R. A. Intestinal master transcription factor CDX2 controls chromatin access for partner transcription factor binding. *Mol. Cell Biol.* **33**, 281–292 (2013).
- Merlos-Suarez, A. et al. The intestinal stem cell signature identifies colorectal cancer stem cells and predicts disease relapse. *Cell Stem Cell* **8**, 511–524 (2011).
- Boyer, L. A. et al. Core transcriptional regulatory circuitry in human embryonic stem cells. *Cell* **122**, 947–956 (2005).
- Qi, Z. et al. BMP restricts stemness of intestinal Lgr5(+) stem cells by directly suppressing their signature genes. *Nat. Commun.* **8**, 13824 (2017).
- Verzi, M. P. et al. Differentiation-specific histone modifications reveal dynamic chromatin interactions and partners for the intestinal transcription factor CDX2. *Dev. Cell* **19**, 713–726 (2010).
- Haber, A. L. et al. A single-cell survey of the small intestinal epithelium. *Nature* **551**, 333–339 (2017).
- Moor, A. E. et al. Spatial reconstruction of single enterocytes uncovers broad zonation along the intestinal villus axis. *Cell* **175**, 1156–1167.e15 (2018).
- Yousefi, M., Li, L. & Lengner, C. J. Hierarchy and plasticity in the intestinal stem cell compartment. *Trends Cell Biol.* **27**, 753–764 (2017).
- Tetteh, P. W. et al. Replacement of Lost Lgr5-positive stem cells through plasticity of their enterocyte-lineage daughters. *Cell Stem Cell* **18**, 203–213 (2016).

### Acknowledgements

This research was funded by a grant from the National Institutes of Health (NIH; R01CA190558) to M.P.V. The Verzi laboratory is also supported by the Intestinal Stem Cell Consortium funded by the National Institute of Diabetes and Digestive and Kidney Diseases (NIDDK) and the National Institute of Allergy and Infectious Diseases (NIAID) of the NIH under grant number U01 DK103141. L.C. was supported by New Jersey Commission on Cancer Research grant DFHS18PPC051. N.H.T., S.L., R.P.V. and A.P. were supported by MacMillan Summer Undergraduate Research Fellowships. R. Shivdasani, R. Hart, T. Nakamura and B. Nickels provided helpful discussions. The research was supported by the Genome Editing shared resource of Rutgers Cancer Institute of New Jersey (P30CA072720), next-generation sequencing services of RUCDR, flow cytometry/cell sorting core facility at Environmental and Occupational Health Sciences Institute (EOHSI) and imaging core facility of Human Genetics Institute of New Jersey.



**Author contributions**

L.C. conceived, designed and performed the animal, cellular, molecular, biochemical and bioinformatic experiments; collected and analyzed the data; and wrote the manuscript. N.H.T. contributed to the staining and organoid experiments. R.P.V. contributed to the staining experiments. S.L. and A.P. contributed to the mouse experiments. R.L.F. performed the Diffbind analysis. A.O.P. performed the human SMAD4 ChIP. M.P.V. conceived, designed and supervised the study and wrote the manuscript.

**Competing interests**

The authors declare no competing interests.

**Additional information**

**Supplementary information** is available for this paper at <https://doi.org/10.1038/s41588-019-0384-0>.

**Reprints and permissions information** is available at [www.nature.com/reprints](http://www.nature.com/reprints).

**Correspondence and requests for materials** should be addressed to M.P.V.

**Publisher's note:** Springer Nature remains neutral with regard to jurisdictional claims in published maps and institutional affiliations.

© The Author(s), under exclusive licence to Springer Nature America, Inc. 2019

## Methods

**Mice.** The *Hnf4y*<sup>Crispr</sup> lines were generated by the genome-editing facility (Rutgers Cancer Institute of New Jersey) using the guide RNA acaagaagaagtacacagg. The two resulting strains had identical 4-base pair (bp) deletions in the fourth exon and no phenotypic differences between the two lines, which were subsequently crossed together for later studies. The *Villin-Cre*<sup>ERT2</sup> transgene<sup>28</sup>, *Hnf4a*<sup>fl/fl</sup> (ref. <sup>29</sup>), *Hnf4y*<sup>Crispr/Crispr</sup> and *Smad4*<sup>fl/fl</sup> (ref. <sup>30</sup>) alleles were integrated to generate the conditional compound-mutants and controls. Both HNF4α isoforms (promoters P1 and P2) include the floxed exons<sup>29</sup> used in our model. Experimental mice (8–12 weeks old) were treated with tamoxifen (Sigma T5648) at 50 mg kg<sup>-1</sup> d<sup>-1</sup> by intraperitoneal injection. Histologic analysis, western blot and quantitative PCR (qPCR) were done after four consecutive days of tamoxifen treatment. For RNA-seq analysis, mice were harvested after two or three consecutive days of tamoxifen treatment. For ChIP-seq and MNase–ChIP, mice were analyzed after three consecutive days of tamoxifen treatment. For the BrdU pulse–chase experiment, mice were injected with 1 mg BrdU and 100 mg kg<sup>-1</sup> tamoxifen on the first day and 50 mg kg<sup>-1</sup> tamoxifen on the second day, and were harvested 48 h after the BrdU injection. For the flow cytometry and single-cell RNA-seq experiments, *Hnf4ay*<sup>DKO</sup> mice were injected with 100 mg kg<sup>-1</sup> tamoxifen on the first day and 50 mg kg<sup>-1</sup> tamoxifen on the second day, and were harvested at 48 h and 42 h after the initial tamoxifen injection, respectively. For the histologic analysis and single-cell RNA-seq experiments of *Hnf4a*<sup>KO</sup>; *Smad4*<sup>KO</sup>, mice were harvested 10 d after the initial tamoxifen treatment. All mouse protocols and experiments were approved by the Rutgers Institutional Animal Care and Use Committee, and we complied with all relevant ethical regulations. All samples were collected between 12:00 and 14:00 to avoid circadian variability.

**Histology and immunostaining.** Intestinal tissues were fixed overnight in 4% paraformaldehyde at 4 °C, washed with PBS, and dehydrated through ascending alcohols before paraffin embedding. Five-micrometer-thick paraffin sections were used for immunohistochemistry and immunofluorescence staining using standard procedures. To mark enterocytes, we detected alkaline phosphatase activity using the AP Staining Kit II (Stemgent). Periodic acid–Schiff (PAS) staining was used to detect goblet cells, and slides were incubated in 0.5% periodic acid and stained with Schiff's Reagent (J612171; Alfa Aesar). Colabeling of goblet cells and BrdU label-retaining cells was performed by BrdU immunohistochemistry and followed by PAS staining. Immunohistochemistry was performed using primary antibodies against HNF4A (Santa Cruz sc-6556 X, 1:2,000), HNF4G (Santa Cruz sc-6558 X, 1:2,000), Ki67 (Abcam ab16667, 1:300), BrdU (Bio-Rad MCA2060, 1:500), Keratin 20 (Cell Signaling 13063, 1:2,500), SMAD4 (Santa Cruz sc-7966, 1:500), MUC2 (Santa Cruz sc-15334, 1:300) and TFF3 (LS-C662731, 1:300; LifeSpan BioSciences). After employing secondary antibody and the Vectastain ABC HRP Kit (Vector Labs), we developed slides using 0.05% 3,3'-diaminobenzidine (DAB, Amresco 0430) and 0.015% hydrogen peroxide in 0.1 M Tris buffer, then counterstained them with hematoxylin. The slides were mounted and viewed on a Nikon Eclipse E800 microscope. Images were photographed with a Retiga 1300 CCD (charge-coupled device) (QImaging) camera and QCapture imaging software. A Zeiss Axiovert 200 M fluorescence microscope was used for imaging the immunofluorescence staining of p-SMAD1/5/9 (Cell Signaling 13820, 1:200) by using a Retiga-SRV CCD (QImaging). Leica TCS SP8 Spectral Confocal System with Lightning Confocal Super Resolution was used for imaging the immunofluorescence staining of HNF4A (Abcam ab41898, 1:100) and HNF4G (Santa Cruz sc-6558 X, 1:100). A Zeiss LSM 510 Meta confocal microscope was used for imaging the immunofluorescence staining of HNF4A (Abcam ab41898, 1:100) and SMAD4 (Cell Signaling 46535, 1:100). ImageJ and Adobe Photoshop were used to adjust contrast and brightness. When adjustments were made, they were applied uniformly for comparative images.

**Intestinal epithelium/villus/crypt isolation and single-cell dissociation.** Freshly harvested duodenum was flushed with cold PBS, opened longitudinally, cut into 1-cm pieces, and then rotated in 3 mM EDTA in PBS at 4 °C. The tissue was then vigorously shaken to release the epithelium from underlying muscular tissue, and the supernatant was collected as the whole epithelium fraction; villi were collected from the top of a 70-μm cell strainer while crypts passed through. Cells were pelleted by centrifugation at 170g at 4 °C and then washed by cold PBS. Cell pellets were used for RNA extraction, ChIP or protein extraction for western blot as described in later sections. To dissociate single cells for flow cytometry and single-cell RNA-seq, we further rotated isolated duodenal villi with 5 U ml<sup>-1</sup> Dispase (Stem Cell 07913) and 200 U ml<sup>-1</sup> DNase I (Sigma D4513) at 37 °C for 30 min, and then washed twice with 1% BSA/PBS and filtered with a 40-μm cell strainer.

**Flow cytometry.** Villus cells were isolated and dissociated as described earlier in this article to determine the percentage of goblet cells in the duodenal villi of *Hnf4ay*<sup>DKO</sup> mice (48 h after tamoxifen injection) and their littermate controls. Cells were blocked with TruStain FcX anti-mouse CD16/32 antibody (1 μg per 10<sup>6</sup> cells, BioLegend 101319) for 10 min on ice to prevent nonspecific labeling and were then labeled with Alexa Fluor 647-conjugated anti-CD24 antibody (1:200, BioLegend 101818) and Atto 488-conjugated *Ulex europaeus* lectin (5 μg ml<sup>-1</sup>, Sigma 19337) on ice for 20 min. Dead cells were eliminated using 0.5 μg ml<sup>-1</sup> DAPI, and goblet

cells (UEA-1+CD24<sup>-</sup>)<sup>31,32</sup> were detected with Beckman Coulter Gallios Flow Cytometer. Kaluza analysis 2.1 software was used for flow cytometry data analysis.

**RNA-seq and data analysis.** Epithelial cells were isolated from mouse duodenum, processed for RNA extraction using TRIzol (Invitrogen) according to the manufacturer's instructions, and sequenced using Illumina's TruSeq RNA Library Prep kit v.2. Raw sequencing reads (fastq) were quality checked using fastQC (v.0.11.3) and were further aligned to mouse (mm9) genomes using Tophat2 (v2.1.0) to generate bam files. Cuffquant (v.2.2.1) was used to generate cxb files from bam files. Cuffnorm (v.2.2.1) was performed to calculate the fragments per kilobase of transcript per million mapped reads (FPKM) using quartile normalization. Cuffdiff<sup>33</sup> (v.2.2.1) was applied to identify differentially expressed genes between the control and the mutants using quartile normalization and per-condition dispersion. Genes with FPKM > 1 were used for further analysis. Cuffdiff was used to generate the preranked gene list. Gene set enrichment analysis (GSEA v.3.0) was performed on the preranked gene list as described previously<sup>34</sup>. Heatmapper<sup>35</sup> was used to display relative transcript levels of genes of interest by using normalized FPKM values from Cuffnorm. Gene ontology analysis was performed with DAVID (v.6.8).

**Single-cell RNA-seq and data analysis.** Single-cell RNA libraries were generated using the Chromium Single Cell 3' v.2 kit (10X Genomics). In brief, each sample of dissociated duodenal villi was incubated with Dead Cell Removal MicroBeads (Miltenyi) and passed through a magnetic column, removing the majority of dead cells/debris. The remaining live cells were counted using a trypan blue exclusion count assay with a hemocytometer and were diluted for loading onto the Chromium Controller. Loading was performed to target capture of ~3,000 gel beads per sample for downstream analysis, and samples were processed through the Chromium Controller following the standard manufacturer's specifications. The sequencing library was validated on the Agilent TapeStation (Agilent Technologies) and quantified with Qubit 2.0 Fluorometer (Invitrogen) and qPCR (Applied Biosystems). The sequencing library was clustered on three lanes of the flow cell. After clustering, the flow cells were loaded on the Illumina HiSeq instrument according to the manufacturer's instructions. The samples were sequenced following 10X Genomics single-cell RNA-sequencing protocols. Image analysis and base calling were conducted by the HiSeq Control Software (HCS v.3.4.0). Raw sequence data (.bcl files) generated from Illumina HiSeq were converted into fastq files and de-multiplexed using the 10X Genomics' cellranger (v.2.1.1) mkfastq command. Subsequent unique molecular identifiers (UMI) and cell barcode de-convolution was performed using 10X Genomics' cellranger count command to generate the final digital gene expression matrices, *t*-distributed stochastic neighbor embedding (*t*-SNE) plot and cloupe files. Single-cell RNA library preparations, sequencing reactions and initial bioinformatics analysis were conducted at GENEWIZ, LLC. Loupe Cell Browser 2.0.0 was used for downstream analysis of goblet cell and enterocyte-enriched genes in each genotype. Plots showing individual gene expression intensity are based on a log<sub>2</sub> scale of the gene expression; the plot of WT cells was reflected over the vertical axis to position the goblet cell cluster for better comparison with knockout (KO) samples.

**Chromatin immunoprecipitation (ChIP) and ChIP-seq.** Standard procedures were used for ChIP, as described previously<sup>36</sup>, with minor modifications on mouse duodenal epithelial cells. For HNF4A and HNF4G ChIP of mouse duodenal epithelium, cells were isolated as described earlier in this article and then cross-linked in 1% formaldehyde (Sigma F8775) for 10 min at 4 °C and then for 35 or 50 min at room temperature. For SMAD4 ChIP of mouse duodenal epithelium, cells were cross-linked in 2 mM DSG (Thermo 20593) for 45 min and then further cross-linked in 1% formaldehyde for 20 min at room temperature. Cells were washed with ice-cold PBS, resuspended with lysis buffer (1% SDS, 10 mM EDTA, pH 8.0, 50 mM Tris, pH 8.0, and protease inhibitor cocktails), and further incubated at room temperature for 10 min. Cell lysates were sonicated using a Diagenode Bioruptor to generate 200- to 500-bp fragments, as determined by agarose gel electrophoresis. The supernatant of lysates was diluted in binding buffer (20 mM Tris, pH 8.0, 2 mM EDTA, pH 8.0, 150 mM NaCl, 1% Triton X-100 and protease inhibitor cocktails) and incubated with HNF4A (6 μg, Santa Cruz sc-6556 X, lot B1015), HNF4G (6 μg, Santa Cruz sc-6558 X, lot F0310) or SMAD4 (20 μl, Cell Signaling 46535, lot 2) antibody coupled to Dynabeads (Invitrogen) at 4 °C overnight. The final concentrations of SDS in the sonicates for mouse HNF4A and SMAD4 ChIP are 0.125% and 0.167%, respectively. The immunoprecipitates were washed five times and rotated at 4 °C with radioimmunoprecipitation assay (RIPA) buffer (50 mM HEPES, pH 7.6, 1 mM EDTA, pH 8.0, 0.7% Na-deoxycholate, 1% NP-40 and 0.5 M LiCl) and a quick wash of TE buffer (0.1 mM EDTA, pH 8.0, and 10 mM Tris, pH 8.0). To recover the DNA, we incubated the samples overnight in reverse cross-linking buffer (1% SDS and 0.1 M NaHCO<sub>3</sub>) at 65 °C. The DNA was purified by QIAquick PCR Purification Kit (QIAGEN) and quantified with PicoGreen (Life Technologies). ChIP enrichment was confirmed with qPCR for putative targets before library preparation. For ChIP-seq, 5 ng each of ChIP or input DNA was used to prepare ChIP-seq libraries with a Rubicon Genomics ThruPLEX DNA-seq Kit (Illumina).

Fragment size was selected with Pippin Prep and sequenced on Illumina HiSeq 2500 or NextSeq 550.

For MNase–ChIP, mouse duodenal epithelial cells were resuspended in digestion buffer (50 mM Tris–HCl, pH 7.6, 1 mM CaCl<sub>2</sub>, 0.2% Triton X-100, 5 mM Na butyrate and protease inhibitor cocktails) and treated with MNase (Sigma N3755) at 0.67 U ml<sup>-1</sup> for 5 min at 37°C. The reaction was terminated by adding 5 mM EDTA in 10 mM Tris, pH 7.6, and samples were dialyzed in chromatin RIPA buffer (10 mM Tris, pH 7.6, 1 mM EDTA, 0.1% SDS, 0.1% Na-deoxycholate and 1% Triton X-100) before the overnight immunoprecipitation (IP) at 4°C with antibody to histone H3K27ac (Abcam ab4729, lot GR184332-2). IP material was subsequently handled as described earlier for conventional ChIP of sonicated genomic DNA (a final concentration of 0.13% SDS in the sonicates).

To perform SMAD4 ChIP in Caco-2 cells, we produced lentiviral vectors by transfecting HEK293-FT cells with the viral packaging constructs (VSVG and Delta 8.2) and plasmids with expression constructs. Caco-2 cells were then transduced serially with lentiviral vectors carrying avi-tagged SMAD4 expression constructs (pReceiver-Lv108; GeneCopoeia) with puromycin resistance cassette and BirA expression plasmid with hygromycin B (Addgene plasmid 29649). Caco-2 cells were cultured in DMEM (Gibco 11995-065), containing 10% FBS (Gibco 26140-095) and 1% penicillin and streptomycin (Invitrogen 15140-122). Cells stably expressing both avi-tagged SMAD4 and BirA were selected with medium containing 2 µg ml<sup>-1</sup> puromycin and 0.4 mg ml<sup>-1</sup> hygromycin B, respectively. Cells were fed 24 h before harvest at approximately 95% confluency. Each 100-µl cell pellet was incubated with 1 ml cross-linking solution containing an equal amount of disuccinimidyl glutarate (DSG, Thermo 20593), disuccinimidyl suberate (DSS, Thermo 21655) and ethylene glycol bis(succinimidyl succinate) (EGS, Thermo 21565), creating a final concentration of 2 mM N-hydroxysuccinimide (NHS) ester (reactive groups). Cells were rocked for 20 min at room temperature, after which fresh formaldehyde was added to make a concentration of 1.22% formaldehyde. The cells were then rocked for an additional 20 min. The cross-linking reaction was stopped with 125 mM glycine. The cells were then washed with PBS, and nuclei were extracted using a Dounce homogenizer and Farnham lysis buffer (5 mM PIPES, pH 8.0, 85 mM KCl, 0.5% NP-40 and protease inhibitor cocktails). IP material was subsequently handled as described earlier for conventional ChIP of sonicated genomic DNA (a final concentration of 0.2% SDS in the sonicates). The diluted sonicates were then incubated with preblocked (0.5% BSA/PBS) streptavidin beads (Invitrogen) overnight at 4°C. The beads were serially washed in low salt (0.1% SDS, 0.1% sodium deoxycholate, 1% Triton X-100, 150 mM NaCl, 1 mM EDTA and 20 mM HEPES, pH 8.0), high salt (0.1% SDS, 0.1% sodium deoxycholate, 1% Triton X-100, 500 mM NaCl, 1 mM EDTA and 20 mM HEPES, pH 8.0), LiCl buffer (250 mM LiCl, 0.5% sodium deoxycholate, 0.5% NP-40, 1 mM EDTA and 20 mM HEPES, pH 8.0) and a final wash buffer (1 mM EDTA and 20 mM HEPES, pH 8.0). The beads were then incubated at 65°C for 6 h in reverse cross-linking buffer (0.1 mM NaHCO<sub>3</sub> and 1% SDS).

**ATAC-seq.** Duodenal villi were treated with prewarmed 0.25% trypsin for 8 min at 37°C on a vortex station (speed set between 6 and 7), neutralized with 10% FBS, and passed through a 40-µm cell strainer to obtain single cells. A total of 50,000 cells were used for ATAC-seq as described previously<sup>37,38</sup> with slight modifications. In brief, cells were centrifuged at 500g for 5 min at 4°C and resuspended in ice-cold lysis buffer (10 mM Tris, pH 7.4, 10 mM NaCl, 3 mM MgCl<sub>2</sub> and 0.1% NP-40). Cells were then centrifuged at 500g for 10 min at 4°C. The isolated nuclear pellets were incubated with a 50-µl reaction of Nextera Tn5 Transposase (Illumina FC-121-1030) for 30 min at 37°C. The transposed chromatin was purified with QIAquick PCR Purification Kit (QIAGEN), and PCR was amplified with high-fidelity 2× PCR Master Mix (New England Biolabs M0541). The optimum number of additional cycles was based on one-third of the maximum fluorescence intensity. The PCR-amplified libraries were purified. Fragment size was selected using Pippin Prep and sequenced on Illumina NextSeq 550.

**Data analysis of ChIP-seq and ATAC-seq.** FastQC (v.0.11.3) was used to check the quality of raw sequencing reads (fastq), and bowtie2 (v.2.2.6) was used to align the sequences to mouse (mm9) or human (hg19) genomes and generate bam files. Deeptools bamCoverage<sup>39</sup> (v.2.4.2, duplicate reads ignored, RPKM normalized and extended reads) was used to generate bigwig files from bam files. BigWigMerge (v.2) was used to merge the bigwig files of different replicates. The Integrative Genomics Viewer<sup>40</sup> (IGV 2.4.13) was used to visualize normalized bigwig tracks. Model-based Analysis of ChIP-Seq<sup>41</sup> (MACS 1.4.1) was used for peak calling and to generate bed files from aligned reads. The shiftsize parameter used in MACS was based on the fragment size of Pippin Prep. HNF4A and HNF4G ChIP-seq of mouse duodenal epithelium were at a *P* value of 10<sup>-3</sup>; SMAD4 ChIP-seq of mouse duodenal epithelium is at a *P* value of 10<sup>-5</sup>; H3K27ac MNase–ChIP-seq and ATAC-seq of mouse duodenal epithelium or villi are at a *P* value of 10<sup>-5</sup>; HNF4A and SMAD4 ChIP-seq of Caco-2 cells are at a *P* value of 10<sup>-5</sup> or 10<sup>-10</sup>. BEDTools<sup>42</sup> (v.2.17.0) was used to merge, intersect or subtract the intervals of bed files. *k*-Means clustering heat maps of ChIP-seq were created with Haystack<sup>43</sup> (v.0.4.0) quantile normalized bigwigs using computeMatrix and plotHeatmap

from deeptools<sup>39</sup> (v.2.4.2). Genomic regions of desired *k*-means clusters were extracted from bed files generated by plotHeatmap. DiffBind<sup>45,44</sup> (v.1.16.3) was used to identify differential signals of HNF4A and HNF4G ChIP-seq, and 0.05 was used as the cutoff for significance. Subsequent analysis of HNF4-binding sites consists of all peaks at MACS *P* value ≤ 10<sup>-3</sup> in each of the four WT replicates merged into a set of 7,287 binding regions. Promoters were defined as bed regions within 2 kb of the transcription start sites (TSSs) of RefSeq genes, whereas enhancers were defined by excluding promoters and were used for subsequent analysis. SitePro<sup>45</sup> (v.1.0.2) was used to compare the average signal profiles of H3K27ac between WT littermate controls and *Hnf4a*<sup>DKO</sup> around HNF4 bound sites. The Peak2gene/BETA-minus function (v.1.0.2) in Cistrome tools<sup>46</sup> was used to identify genes within 10, 20 or 30 kb of HNF4-bound sites, and gene ontology term analysis (DAVID v.6.8)<sup>47</sup> was used for functional annotation of those genes. HOMER findMotifsGenome.pl<sup>48</sup> (v.4.8.3, HOMER de novo results) was used to call transcription factor motifs enriched at peaks. All analysis was done with publicly available algorithms, and additional details are available from the corresponding author on request.

**qPCR with reverse transcription.** cDNA was synthesized from total RNA with Oligo(dT)<sub>20</sub> primers using SuperScript III First-Strand Synthesis SuperMix (Invitrogen). qPCR with reverse transcription (qRT–PCR) was performed to measure changes in mRNA expression using Applied Biosystems 7900HT Sequence Detection System. The sequences of the primers used are available on request. In brief, the qRT–PCR was carried out using Power SYBR Green PCR Master Mix, and the amplification conditions were as follows: 50°C for 2 min, 95°C for 10 min, followed by 40 cycles of 95°C for 15 s and 60°C for 1 min. Hypoxanthine-guanine phosphoribosyl transferase 1 (*Hprt1*) was used as an internal control. The 2<sup>-ΔΔC<sub>t</sub></sup> method was applied to calculate the fold change of the relative transcript level.

**Protein extraction and western blotting.** The protein of duodenal epithelium or intestinal organoids was extracted with RIPA buffer (50 mM Tris–HCl, pH 8.0, 150 mM NaCl, 1% NP-40, 0.5% Na-deoxycholate, 0.1% SDS, protease inhibitor cocktails and phosphatase inhibitors). The nuclear protein extraction of duodenal villi was performed as described previously<sup>49</sup>. Four cycles and two cycles of Bioruptor sonication (30 s on and 30 s off) were used before and after rotating cells in lysis buffer at 4°C for 30 min, respectively. Protein concentration was determined by Pierce BCA Protein Assay Kit (Thermo). Immunodetection was performed using specific antibodies against HNF4A (Santa Cruz sc-6556 X, 1:1,000), HNF4G (Santa Cruz sc-6558 X, 1:1,000), Lamin B1 (Abcam ab16048, 1:1,000), GAPDH (Santa Cruz sc-25778, 1:5,000), β-actin (Abcam ab8227, 1:5,000) and SMAD1/5/9 Antibody Sampler Kit (Cell Signaling 12656, 1:1,000).

**Organoid culture.** Primary crypt-derived organoids were isolated from duodenal epithelium and cultured in Cultrex reduced growth factor basement membrane matrix, Type R1 (Trevigen) according to established methods<sup>40</sup>. The organoids were treated with 1 µM tamoxifen dissolved in ethanol for 12 h. Vehicle-treated organoids served as a control. Tamoxifen was added into culture medium of organoids on day 2 after seeding. Organoids were imaged using a Zeiss Axiovert 200 M inverted microscope with a Retiga-SRV CCD (QImaging). For BMP2 and Noggin treatment experiments, recombinant BMP2 (R&D 355-BM) and Noggin (PeproTech 250-38) were prepared according to the supplier's instructions, and vehicle controls were used in organoid culture. The organoids were harvested on day 6 for subsequent RNA or protein extraction. QIAGEN RNeasy Micro Kit was used to extract RNA from organoids.

**Statistical analysis.** The data are presented as mean ± s.e.m., and statistical comparisons were performed using one-way analysis of variance (ANOVA) followed by Dunnett's posttest with the GraphPad Prism v.7.02 or two-sided Student's *t*-test at \*\*\**P* < 0.001, \*\**P* < 0.01 or \**P* < 0.05. The exact *P* values are shown in Supplementary Table 4. Mann–Whitney *U*-test and Kruskal–Wallis test (followed by post hoc Dunn's test) were used as part of RNA-seq analysis. Bioinformatics-related statistical analysis was done with the embedded statistics in each package, including DiffBind<sup>45</sup>, HOMER<sup>48</sup>, Cuffdiff<sup>53</sup>, GSEA<sup>34,51</sup> and DAVID<sup>47</sup>. *P* < 0.05 (95% confidence interval) was considered statistically significant.

**Reporting Summary.** Further information on research design is available in the Nature Research Reporting Summary linked to this article.

## Data availability

All RNA-seq, ChIP-seq and ATAC-seq data of this study have been deposited in GEO (GSE112946). The following datasets from GEO were reanalyzed with our sequencing data: the accession numbers for the transcriptome of *Smad4*<sup>KO</sup> and HNF4A ChIP in Caco-2 cells from our previous studies are GSE102171 (ref. <sup>52</sup>) and GSE23436 (ref. <sup>23</sup>), respectively. GSE51336 (ref. <sup>7</sup>) and GSE36025 (ref. <sup>14</sup>) were used to analyze chromatin accessibility and RNA-seq data across different tissues. GSE57919 (ref. <sup>53</sup>) and GSE98724 (ref. <sup>54</sup>) were used to mark active chromatin. GSE53545, GSE70766 (ref. <sup>55</sup>) and GSE102171 (ref. <sup>52</sup>) were used to perform RNA-seq analysis of villus-enriched genes and crypt-enriched genes.



## References

28. el Marjou, F. et al. Tissue-specific and inducible Cre-mediated recombination in the gut epithelium. *Genesis* **39**, 186–193 (2004).
29. Hayhurst, G. P., Lee, Y. H., Lambert, G., Ward, J. M. & Gonzalez, F. J. Hepatocyte nuclear factor 4alpha (nuclear receptor 2A1) is essential for maintenance of hepatic gene expression and lipid homeostasis. *Mol. Cell Biol.* **21**, 1393–1403 (2001).
30. Yang, X., Li, C., Herrera, P. L. & Deng, C. X. Generation of Smad4/Dpc4 conditional knockout mice. *Genesis* **32**, 80–81 (2002).
31. Wong, V. W. et al. Lrig1 controls intestinal stem-cell homeostasis by negative regulation of ErbB signalling. *Nat. Cell Biol.* **14**, 401–408 (2012).
32. Jadhav, U. et al. Dynamic reorganization of chromatin accessibility signatures during dedifferentiation of secretory precursors into Lgr5+ intestinal stem cells. *Cell Stem Cell* **21**, 65–77.e5 (2017).
33. Trapnell, C. et al. Differential gene and transcript expression analysis of RNA-seq experiments with TopHat and Cufflinks. *Nat. Protoc.* **7**, 562–578 (2012).
34. Subramanian, A. et al. Gene set enrichment analysis: a knowledge-based approach for interpreting genome-wide expression profiles. *Proc. Natl Acad. Sci. USA* **102**, 15545–15550 (2005).
35. Babicki, S. et al. Heatmapper: web-enabled heat mapping for all. *Nucl. Acids Res.* **44**, W147–W153 (2016).
36. Perekatt, A. O. et al. YY1 is indispensable for Lgr5+ intestinal stem cell renewal. *Proc. Natl Acad. Sci. USA* **111**, 7695–7700 (2014).
37. Buenrostro, J. D., Wu, B., Chang, H. Y. & Greenleaf, W. J. ATAC-seq: a method for assaying chromatin accessibility genome-wide. *Curr. Protoc. Mol. Biol.* **109**, 21.29.1–21.29.9 (2015).
38. Buenrostro, J. D., Giresi, P. G., Zaba, L. C., Chang, H. Y. & Greenleaf, W. J. Transposition of native chromatin for fast and sensitive epigenomic profiling of open chromatin, DNA-binding proteins and nucleosome position. *Nat. Methods* **10**, 1213–1218 (2013).
39. Ramirez, F. et al. deepTools2: a next generation web server for deep-sequencing data analysis. *Nucl. Acids Res.* **44**, W160–W165 (2016).
40. Robinson, J. T. et al. Integrative genomics viewer. *Nat. Biotechnol.* **29**, 24–26 (2011).
41. Zhang, Y. et al. Model-based analysis of ChIP-Seq (MACS). *Genome Biol.* **9**, R137 (2008).
42. Quinlan, A. R. BEDTools: the Swiss-Army tool for genome feature analysis. *Curr. Protoc. Bioinformatics* **47**, 11.12.1–11.12.34 (2014).
43. Pinello, L., Farouni, R. & Yuan, G. C. Haystack: systematic analysis of the variation of epigenetic states and cell-type specific regulatory elements. *Bioinformatics* **34**, 1930–1933 (2018).
44. Ross-Innes, C. S. et al. Differential oestrogen receptor binding is associated with clinical outcome in breast cancer. *Nature* **481**, 389–393 (2012).
45. Shin, H., Liu, T., Manrai, A. K. & Liu, X. S. CEAS: cis-regulatory element annotation system. *Bioinformatics* **25**, 2605–2606 (2009).
46. Liu, T. et al. Cistrome: an integrative platform for transcriptional regulation studies. *Genome Biol.* **12**, R83 (2011).
47. Huang da, W., Sherman, B. T. & Lempicki, R. A. Systematic and integrative analysis of large gene lists using DAVID bioinformatics resources. *Nat. Protoc.* **4**, 44–57 (2009).
48. Heinz, S. et al. Simple combinations of lineage-determining transcription factors prime cis-regulatory elements required for macrophage and B cell identities. *Mol. Cell* **38**, 576–589 (2010).
49. Shaked, H., Guma, M. & Karin, M. Analysis of NF-kappaB activation in mouse intestinal epithelial cells. *Method. Mol. Biol.* **1280**, 593–606 (2015).
50. Sato, T. et al. Single Lgr5 stem cells build crypt-villus structures in vitro without a mesenchymal niche. *Nature* **459**, 262–265 (2009).
51. Tamayo, P., Steinhardt, G., Liberzon, A. & Mesirov, J. P. The limitations of simple gene set enrichment analysis assuming gene independence. *Stat. Methods Med. Res.* **25**, 472–487 (2016).
52. Perekatt, A. O. et al. SMAD4 suppresses WNT-driven dedifferentiation and oncogenesis in the differentiated gut epithelium. *Cancer Res.* **78**, 4878–4890 (2018).
53. Camp, J. G. et al. Microbiota modulate transcription in the intestinal epithelium without remodeling the accessible chromatin landscape. *Genome Res.* **24**, 1504–1516 (2014).
54. Saxena, M. et al. Transcription factor-dependent 'anti-repressive' mammalian enhancers exclude H3K27me3 from extended genomic domains. *Gene. Dev.* **31**, 2391–2404 (2017).
55. San Roman, A. K., Tovaglieri, A., Breault, D. T. & Shivdasani, R. A. Distinct processes and transcriptional targets underlie CDX2 requirements in intestinal stem cells and differentiated villus cells. *Stem Cell Rep.* **5**, 673–681 (2015).

# Reporting Summary

Nature Research wishes to improve the reproducibility of the work that we publish. This form provides structure for consistency and transparency in reporting. For further information on Nature Research policies, see [Authors & Referees](#) and the [Editorial Policy Checklist](#).

## Statistics

For all statistical analyses, confirm that the following items are present in the figure legend, table legend, main text, or Methods section.

- |                                     |  |
|-------------------------------------|--|
| n/a                                 | Confirmed  |
| <input type="checkbox"/>            | <input checked="" type="checkbox"/> The exact sample size ( $n$ ) for each experimental group/condition, given as a discrete number and unit of measurement  |
| <input type="checkbox"/>            | <input checked="" type="checkbox"/> A statement on whether measurements were taken from distinct samples or whether the same sample was measured repeatedly  |
| <input type="checkbox"/>            | <input checked="" type="checkbox"/> The statistical test(s) used AND whether they are one- or two-sided<br><i>Only common tests should be described solely by name; describe more complex techniques in the Methods section.</i>   |
| <input checked="" type="checkbox"/> | <input type="checkbox"/> A description of all covariates tested  |
| <input type="checkbox"/>            | <input checked="" type="checkbox"/> A description of any assumptions or corrections, such as tests of normality and adjustment for multiple comparisons  |
| <input type="checkbox"/>            | <input checked="" type="checkbox"/> A full description of the statistical parameters including central tendency (e.g. means) or other basic estimates (e.g. regression coefficient) AND variation (e.g. standard deviation) or associated estimates of uncertainty (e.g. confidence intervals) |
| <input type="checkbox"/>            | <input checked="" type="checkbox"/> For null hypothesis testing, the test statistic (e.g. $F$ , $t$ , $r$ ) with confidence intervals, effect sizes, degrees of freedom and $P$ value noted<br><i>Give <math>P</math> values as exact values whenever suitable.</i>                            |
| <input checked="" type="checkbox"/> | <input type="checkbox"/> For Bayesian analysis, information on the choice of priors and Markov chain Monte Carlo settings  |
| <input checked="" type="checkbox"/> | <input type="checkbox"/> For hierarchical and complex designs, identification of the appropriate level for tests and full reporting of outcomes  |
| <input checked="" type="checkbox"/> | <input type="checkbox"/> Estimates of effect sizes (e.g. Cohen's $d$ , Pearson's $r$ ), indicating how they were calculated  |

Our web collection on [statistics for biologists](#) contains articles on many of the points above.

## Software and code

Policy information about [availability of computer code](#)

### Data collection

QCapture imaging software (v2.0.8)  
HiSeq Control Software (v3.4.0)  
ABI 7900HT Sequence Detection Systems (v2.1.1)  
Gallios Cytometry List Mode Data Acquisition and Analysis Software (v1.2)

### Data analysis

FastQC (v0.11.3)  
Tophat2 (v2.1.0)  
Cuffquant (v2.2.1)  
Cuffnorm (v2.2.1)  
Cuffdiff (v2.2.1)  
Gene set enrichment analysis (GSEA v3.0)  
DAVID (v6.8)  
Heatmapper (<http://www.heatmapper.ca/expression/>)  
Bowtie2 (v2.2.6)  
DeepTools (v2.4.2)  
BigWigMerge (v2)  
Integrative Genomics Viewer (IGV 2.4.13)  
Model-based Analysis of ChIP-Seq (MACS 1.4.1)  
BEDTools (v2.17.0)  
Haystack (v0.4.0)  
DiffBind (v1.16.3)  
SitePro (v1.0.2)  
Peak2gene/BETA-minus (v1.0.0)  
Homer findMotifsGenome.pl (v4.8.3)  
Cellranger (v2.1.1)

Loupe Cell Browser (v2.0.0)  
 Kaluza analysis (v2.1)  
 GraphPad Prism (v7.02)  
 ImageJ (v1.51j8)  
 Adobe Photoshop (v12.0.1)

For manuscripts utilizing custom algorithms or software that are central to the research but not yet described in published literature, software must be made available to editors/reviewers. We strongly encourage code deposition in a community repository (e.g. GitHub). See the Nature Research [guidelines for submitting code & software](#) for further information.

## Data

Policy information about [availability of data](#)

All manuscripts must include a [data availability statement](#). This statement should provide the following information, where applicable:

- Accession codes, unique identifiers, or web links for publicly available datasets
- A list of figures that have associated raw data
- A description of any restrictions on data availability

All RNA-seq, ChIP-seq and ATAC-seq data of this study have been deposited in GEO (GSE112946).

## Field-specific reporting

Please select the one below that is the best fit for your research. If you are not sure, read the appropriate sections before making your selection.

☒ Life sciences ☐ Behavioural & social sciences ☐ Ecological, evolutionary & environmental sciences

For a reference copy of the document with all sections, see [nature.com/documents/nr-reporting-summary-flat.pdf](https://nature.com/documents/nr-reporting-summary-flat.pdf)

## Life sciences study design

All studies must disclose on these points even when the disclosure is negative.

Sample size	The sample sizes are determined based on widely used and accepted methods, based on the minimal amount of mice required to detect significance in a standardly powered experiment.
Data exclusions	In RNA-seq analysis, genes with FPKM>1 (a commonly used minimal expression threshold) were used for further analysis. ENCODE blacklisted regions were excluded in Caco-2 ChIP-seq, which is a standard protocol in ChIP-seq analysis. When reanalyzing the public datasets from GEO, principal component analysis and hierarchical clustering were performed as quality control, and one outlier was omitted from further analysis. All the exclusion criteria were pre-established by previous studies of ours and others.
Replication	All attempts at replication were successful.
Randomization	Mice with needed genotypes and ages were chosen randomly. Mice were treated equally. We use littermates (if possible) and at least cagemates for all mouse studies.
Blinding	For animal studies, people who performed the experiments did not know the exact genotypes/treatment until after data were analyzed. In some cases, the phenotype was apparent by macroscopic tissue appearance and thus blinding was not possible. Tissue culture experiments were not blinded.

## Reporting for specific materials, systems and methods

We require information from authors about some types of materials, experimental systems and methods used in many studies. Here, indicate whether each material, system or method listed is relevant to your study. If you are not sure if a list item applies to your research, read the appropriate section before selecting a response.

### Materials & experimental systems

n/a	Involved in the study
<input type="checkbox"/>	<input checked="" type="checkbox"/> Antibodies
<input type="checkbox"/>	<input checked="" type="checkbox"/> Eukaryotic cell lines
<input checked="" type="checkbox"/>	<input type="checkbox"/> Palaeontology
<input type="checkbox"/>	<input checked="" type="checkbox"/> Animals and other organisms
<input checked="" type="checkbox"/>	<input type="checkbox"/> Human research participants
<input checked="" type="checkbox"/>	<input type="checkbox"/> Clinical data

### Methods

n/a	Involved in the study
<input type="checkbox"/>	<input checked="" type="checkbox"/> ChIP-seq
<input type="checkbox"/>	<input checked="" type="checkbox"/> Flow cytometry
<input checked="" type="checkbox"/>	<input type="checkbox"/> MRI-based neuroimaging

## Antibodies

Antibodies used

Immunohistochemistry was performed using primary antibodies against Hnf4α (clone C19, Santa Cruz sc-6556 X, lot B1015,



1:2000), Hnf4 $\gamma$  (clone C18, Santa Cruz sc-6558 X, lot F0310, 1:2000), Ki67 (clone SP6, Abcam ab16667, lot GR289011-8, 1:300), BrdU (clone BU1/75, Bio-Rad MCA2060, lot 1015, 1:500), Keratin 20 (clone D9Z1Z, Cell Signaling 13063, lot 1, 1:2500), Smad4 (clone B-8, Santa Cruz sc-7966, lot A2816, 1:500), Muc2 (clone H-300, Santa Cruz sc-15334, 1:300) and Tff3 (LifeSpan BioSciences, LS-C662731, lot 127590, 1:300). Hnf4 $\alpha$  (clone K9218, Abcam ab41898, lot GR4841-58, 1:100), Hnf4 $\gamma$  (clone C18, Santa Cruz sc-6558 X, lot F0310 1:100), Smad4 (clone D3R4N, Cell signaling 46535, lot 2, 1:100) and pSmad1/5/9 (clone D5B10, Cell Signaling 13820, lot 3, 1:200) were used for immunofluorescence staining. Western blot was performed using specific antibodies against Hnf4 $\alpha$  (clone C19, Santa Cruz sc-6556 X, lot B1015, 1:1000), Hnf4 $\gamma$  (clone C18, Santa Cruz sc-6558 X, lot F0310, 1:1000), Lamin B1 (Abcam ab16048, 1:1000), GAPDH (clone FL-335, Santa Cruz sc-25778, lot D0612, 1:5000),  $\beta$ -actin (Abcam ab8227, lot GR3197625-1, 1:5000), and Smad 1/5/9 Antibody Sampler Kit (Cell signaling 12656) including Phospho-Smad1 (clone D40B7, Cell Signaling 5753, lot 3, 1:1000), Phospho-Smad1/5 (clone 41D10, Cell Signaling 9516, lot 9, 1:1000), Phospho-Smad1/5/9 (clone D5B10, Cell Signaling 13820, lot 3, 1:1000), Smad 1 (clone D59D7, Cell Signaling 6944, lot 5, 1:1000), Smad 4 (clone D3M6U, Cell Signaling 38454, lot 2, 1:1000) and Smad 5 (clone D4G2, Cell Signaling 12534, lot 2, 1:1000). Hnf4 $\alpha$  (clone C19, Santa Cruz sc-6556 X, lot B1015, 6  $\mu$ g), Hnf4 $\gamma$  (clone C18, Santa Cruz sc-6558 X, lot F0310, 6  $\mu$ g), Smad4 (clone D3R4N, Cell signaling 46535, lot 2, 20  $\mu$ l) and Histone H3K27ac (clone H3 aa 1-100, Abcam ab4729, lot GR184332-2, 6  $\mu$ g) antibodies were used for ChIP-seq. TruStain FcX™ anti-mouse CD16/32 (clone 93, BioLegend 101319, lot B247951, 1.0  $\mu$ g per million cells in 100  $\mu$ l volume) and Alexa Fluor 647-conjugated CD24 (clone M1/69, BioLegend 101818, lot B263416 1:200) antibodies were used for flow cytometry experiments.

#### Validation

All antibodies are validated for detecting mouse proteins by the manufacturer and all have been cited in many peer-reviewed articles. By Western blot, the specificity of Hnf4 $\alpha$  and Hnf4 $\gamma$  antibodies were determined using single HNF4 knockout mice to establish that there is no cross-reactivity by these antibodies.

## Eukaryotic cell lines

Policy information about [cell lines](#)

#### Cell line source(s)

Caco-2 cell line is a kind gift from Ramesh Shivdasani.

#### Authentication

The recommended tests are described by the ATCC, and the cell line is authenticated by morphological characteristics and differentiation characteristics.

#### Mycoplasma contamination

Our tissue culture facility is tested routinely and has been negative.

#### Commonly misidentified lines (See [ICLAC](#) register)

None of the cell lines used are listed in the ICLAC database.

## Animals and other organisms

Policy information about [studies involving animals](#); [ARRIVE guidelines](#) recommended for reporting animal research

#### Laboratory animals

The Hnf4 $\gamma$ Crispr mouse was generated by the genome editing facility (Rutgers Cancer Institute of New Jersey). The Villin-CreERT2 transgene, Hnf4 $\alpha$ f/f, Hnf4 $\gamma$ Crispr/Crispr and Smad4f/f alleles were integrated to generate the conditional compound-mutants and controls. 8-12 weeks old, same sex (both males and females) mice were used. Tissues were collected at mid-day to minimize circadian differences.

#### Wild animals

The study did not involve wild animals.

#### Field-collected samples

The study did not involve samples collected from the field.

#### Ethics oversight

All mouse protocols and experiments were approved by the Rutgers Institutional Animal Care and Use Committee.

Note that full information on the approval of the study protocol must also be provided in the manuscript.

## ChIP-seq

### Data deposition

☒ Confirm that both raw and final processed data have been deposited in a public database such as [GEO](#).

☒ Confirm that you have deposited or provided access to graph files (e.g. BED files) for the called peaks.

#### Data access links

May remain private before publication.

<https://www.ncbi.nlm.nih.gov/geo/query/acc.cgi?acc=GSE112946>

#### Files in database submission

WT\_Hnf4 $\alpha$ ChIP\_rep1.fastq.gz  
WT\_Hnf4 $\alpha$ ChIP\_rep2.fastq.gz  
WT\_Hnf4 $\gamma$ ChIP\_rep1.fastq.gz  
WT\_Hnf4 $\gamma$ ChIP\_rep2.fastq.gz  
Hnf4 $\alpha$ KO\_Hnf4 $\gamma$ ChIP\_rep1.fastq.gz  
Hnf4 $\alpha$ KO\_Hnf4 $\gamma$ ChIP\_rep2.fastq.gz  
Hnf4 $\gamma$ KO\_Hnf4 $\alpha$ ChIP\_rep1.fastq.gz  
Hnf4 $\gamma$ KO\_Hnf4 $\alpha$ ChIP\_rep2.fastq.gz  
WT\_input DNA.fastq.gz

WT\_Smad4ChIP\_rep1.fastq.gz  
 WT\_Smad4ChIP\_rep2.fastq.gz  
 WT\_DSGFA\_input\_DNA.fastq.gz  
 WT\_H3K27ac\_MNaseChIP\_rep1.fastq.gz  
 WT\_H3K27ac\_MNaseChIP\_rep2.fastq.gz  
 Hnf4αDKO\_H3K27ac\_MNaseChIP\_rep1.fastq.gz  
 Hnf4αDKO\_H3K27ac\_MNaseChIP\_rep2.fastq.gz  
 WT\_Villi\_ATAC-seq.fastq.gz  
 CaCO2\_Avi\_Smad4\_BiotinChIP.fastq.gz  
 Merge\_WT\_Hnf4αChIP.bw  
 Merge\_WT\_Hnf4γChIP.bw  
 WT\_H3K27ac\_MNaseChIP\_rep1.bw  
 WT\_H3K27ac\_MNaseChIP\_rep2.bw  
 Hnf4αDKO\_H3K27ac\_MNaseChIP\_rep1.bw  
 Hnf4αDKO\_H3K27ac\_MNaseChIP\_rep2.bw  
 WT\_Smad4ChIP\_rep1.bw  
 WT\_Smad4ChIP\_rep2.bw  
 WT\_Villi\_ATAC-seq.bw  
 CaCO2\_Avi\_Smad4\_BiotinChIP.bw  
 Merge\_WT\_Hnf4ChIP.bed  
 Merge\_WT\_H3K27ac\_MNaseChIP.bed  
 Merge\_Hnf4αDKO\_H3K27ac\_MNaseChIP.bed  
 Merge\_WT\_Smad4ChIP.bed  
 WT\_Villi\_ATAC-seq.bed  
 CaCO2\_Avi\_Smad4\_BiotinChIP.bed

Genome browser session  
 (e.g. [UCSC](https://genome.ucsc.edu/))

Bigwig files are provided for visualization with the integrative genomics viewer: <https://software.broadinstitute.org/software/igv/>

## Methodology

### Replicates

We used two biological replicates for Hnf4α, Hnf4γ, Smad4 and H3K27ac ChIP-seq. All the information of ChIP-seq replicates used in this study is listed in GSE112946 (GEO).

### Sequencing depth

WT\_Hnf4αChIP\_rep1: 24327533 reads  
 WT\_Hnf4αChIP\_rep2: 12286199 reads  
 WT\_Hnf4γChIP\_rep1: 23690454 reads  
 WT\_Hnf4γChIP\_rep2: 15815907 reads  
 Hnf4αKO\_Hnf4γChIP\_rep1: 24977705 reads  
 Hnf4αKO\_Hnf4γChIP\_rep2: 13147021 reads  
 Hnf4γKO\_Hnf4αChIP\_rep1: 20228670 reads  
 Hnf4γKO\_Hnf4αChIP\_rep2: 34988008 reads  
 WT\_Smad4ChIP\_rep1: 38456230 reads  
 WT\_Smad4ChIP\_rep2: 45758633 reads  
 WT\_H3K27ac\_MNaseChIP\_rep1: 78758016 reads  
 WT\_H3K27ac\_MNaseChIP\_rep2: 72477733 reads  
 Hnf4αDKO\_H3K27ac\_MNaseChIP\_rep1: 76943409 reads  
 Hnf4αDKO\_H3K27ac\_MNaseChIP\_rep2: 70058059 reads  
 WT\_Villi\_ATAC: 62747875 reads  
 CaCO2\_Avi\_Smad4\_BiotinChIP: 31078444 reads

### Antibodies

Hnf4α (clone C19, Santa Cruz sc-6556 X, lot B1015, 6 µg), Hnf4γ (clone C18, Santa Cruz sc-6558 X, lot F0310, 6 µg), Smad4 (clone D3R4N, Cell signaling 46535, lot 2, 20 µl) and Histone H3K27ac (clone H3 aa 1-100, Abcam ab4729, lot GR184332-2, 6 µg) antibodies were used for ChIP-seq.

### Peak calling parameters

Model-based Analysis of ChIP-Seq (MACS 1.4.1) was used for peak calling and to generate bed files from aligned reads. The shiftsize parameter used in MACS was based on the fragment size of Pippin Prep. Hnf4α and Hnf4γ ChIP-seq of mouse duodenal epithelium are at a p-value of 1e-3; Smad4 ChIP-seq, H3K27ac MNase-ChIP-seq and ATAC-seq of mouse duodenal epithelium or villi are at a p-value of 1e-5; Hnf4α and Smad4 ChIP-seq of Caco-2 cells are at a p-value of 1e-5 or 1e-10. WT duodenal epithelium input DNA was used as a control for MACS peak calling.

### Data quality

FastQC (v0.11.3) was used to check the quality of raw sequencing reads (fastq). HNF4 binding sites consists of all peaks at MACS p-value ≤ 1e-3 in each of the 4 wild-type replicates merged into a set of 7287 binding regions. Promoters were defined as bed regions within 2 kb of the transcription start sites of RefSeq genes, whereas enhancers were defined by excluding promoters and used for subsequent analysis. ENCODE blacklisted regions was removed from Caco-2 ChIP-seq binding regions.  
 Merge\_WT\_Hnf4ChIP: 7287 peaks (p-value ≤ 1e-3)  
 Merge\_WT\_H3K27ac\_MNaseChIP: 51955 peaks (p-value ≤ 1e-5)  
 Merge\_Hnf4αDKO\_H3K27ac\_MNaseChIP: 52878 peaks (p-value ≤ 1e-5)  
 Merge\_WT\_Smad4ChIP: 25054 peaks (p-value ≤ 1e-5)  
 WT\_Villi\_ATAC: 48252 peaks (p-value ≤ 1e-5)  
 CaCO2\_Avi\_Smad4\_BiotinChIP: 41300 peaks (p-value ≤ 1e-5)

### Software

FastQC (v0.11.3) was used to check the quality of raw sequencing reads (fastq), and bowtie2 (v2.2.6) was used to align the

## Software

sequences to mouse (mm9) or human (hg19) genomes and generate bam files. Deeptools bamCoverage (v2.4.2, duplicate reads ignored, RPKM normalized and extended reads) was used to generate bigwig files from bam files. BigWigMerge (v2) was used to merge the bigwig files of different replicates. The Integrative Genomics Viewer (IGV 2.4.13) was used to visualize normalized bigwig tracks. Model-based Analysis of ChIP-Seq (MACS 1.4.1) was used for peak calling and to generate bed files from aligned reads. BEDTools (v2.17.0) was used to merge, intersect or subtract the intervals of bed files. k-means clustering heatmaps of ChIP-seq were created with Haystack (v0.4.0) quantile normalized bigwigs using computeMatrix and plotHeatmap from deeptools (v2.4.2). Genomic regions of desired k-means clusters were extracted from bed files generated by plotHeatmap. DiffBind (v1.16.3) was used to identify differential signals of Hnf4 $\alpha$  and Hnf4 $\gamma$  ChIP-seq. SitePro (v1.0.2) was used to compare the average signal profiles of H3K27ac. The Peak2gene/BETA-minus (v1.0.2) function in Cistrome tools was used to identify genes within 10 kb, 20 kb, or 30 kb of HNF4 binding sites, and gene ontology (GO) term analysis (DAVID v6.8) was used for functional annotation of those genes. Homer findMotifsGenome.pl (v4.8.3, homer de novo Results) was used to call transcription factor motifs enriched at peaks.

## Flow Cytometry

### Plots

Confirm that:

- ☒ The axis labels state the marker and fluorochrome used (e.g. CD4-FITC).
- ☒ The axis scales are clearly visible. Include numbers along axes only for bottom left plot of group (a 'group' is an analysis of identical markers).
- ☒ All plots are contour plots with outliers or pseudocolor plots.
- ☒ A numerical value for number of cells or percentage (with statistics) is provided.

### Methodology

#### Sample preparation

Freshly harvested duodenum was flushed with cold PBS, opened longitudinally, cut into 1 cm pieces, and then rotated in 3 mM EDTA in PBS at 4 °C. The tissue was then vigorously shaken to release the epithelium from underlying muscular tissue, and the supernatant was collected as the whole epithelium fraction; villi were collected from the top of a 70- $\mu$ m cell strainer while crypts passed through. Cells were pelleted by centrifugation at 170 g at 4 °C and then washed by cold PBS. To dissociate single cells for flow cytometry, isolated duodenal villi were further rotated with 5U/ml dispase (Stem Cell, #07913) and 200 U/ml of DNase I (Sigma D4513) at 37 °C for 30 min, and were then washed twice with 1% BSA/PBS, and filtered with a 40- $\mu$ m cell strainer.

#### Instrument

Beckman Coulter Gallios Flow Cytometer

#### Software

Gallios Cytometry List Mode Data Acquisition and Analysis Software (v1.2)  
Kaluza Analysis (v2.1)

#### Cell population abundance

The purity of sorted cell purity was >95%, determined by flow-cytometry.

#### Gating strategy

Preliminary FSC/SSC gating was applied to intestinal villus cell population. Dead cells were eliminated using 0.5  $\mu$ g/ml DAPI and goblet cells (UEA-1+CD24-) were gated based on the specific staining as described in Methods. Positive and negative populations were defined and gated by the negative control and single staining control samples.

- ☒ Tick this box to confirm that a figure exemplifying the gating strategy is provided in the Supplementary Information.